Fluxes, Interactions and Environment at the Land-Ocean Boundary. Downscaling, Assimilation and Coupling.
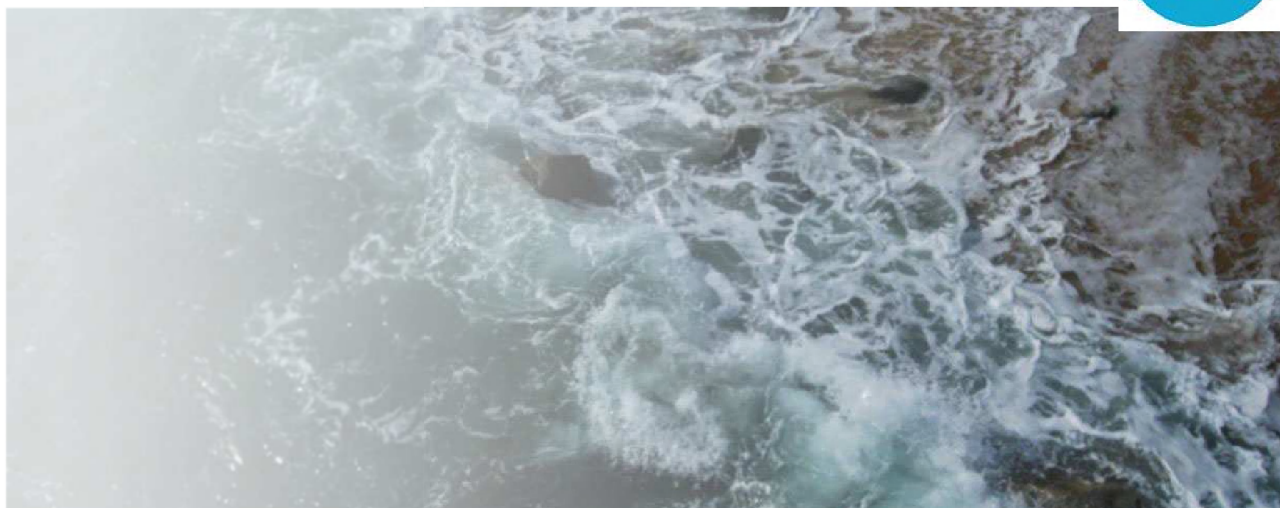
Date: December, 2012

Report Number: D3.3

Due date for deliverable: Month 36

Leader: KUL

Document Dissemination Level: PU

PU   Public

PP   Restricted to other program participants (including the Commission Services)

RE   Restricted to a group specified by the consortium (including the Commission Services)

CO   Confidential, only for members of the consortium (including the Commission Services)

DOCUMENT INFORMATION

Title	Impact assessment for the improved four boundary conditions (at bed, free-surface, land-boundary and offshore-boundary) on coastal hydrodynamics and particulate transport.
Lead Author	Maria Liste,
Contributors	Jaak Monbaliu, Manel Grifoll, Ingrid Keupers, Erik Toorman, Qilong Bi Albert Soret, Juan Fernández, Sandro Carniel, Alvise Benetazzo, Joanna Staneva, Katrin Wahle, Lucy Bricheno, Judith Wolf, Jeremy Lepesqueur, Fabrice Ardhuin.
Distribution	
Document Reference	Report_D3.3

DOCUMENT HISTORY

Date	Revision	Prepared by	Organization	Approved by	Notes
10-2012	1	Maria Liste	KUL		First draft

ACKNOWLEDGEMENT

DISCLAIMER

This document reflects only the authors' views and not those of the European Community. This work may rely on data from sources external to the FIELD_AC project Consortium. Members of the Consortium do not accept liability for loss or damage suffered by any third party as a result of errors or inaccuracies in such data. The information in this document is provided "as is" and no guarantee or warranty is given that the information is fit for any particular purpose. The user thereof uses the information at its sole risk and neither the European Community nor any member of the FIELD_AC Consortium is liable for any use that may be made of the information.

Table of Contents

List of Figures

List of Tables

Summary

The FIELD_AC project aims at providing an improved operational service for coastal areas and at generating added value for shelf and regional scale predictions. Coastal-zone oceanographic predictions seldom appraise the land discharge as a boundary condition. River fluxes are sometimes considered, but neglecting their 3D character, while the "distributed" continental run-off is not taken into consideration. Moreover, many coastal scale processes, particularly those relevant in geographically restricted domains (coasts with harbors or river mouth areas), are not well parameterized in present simulations.

Work Package 3 dedicated to Boundary Fluxes aims to establish and use the best possible boundary conditions for coastal water quality modelling. On this scale, all boundaries become important. For the land boundary side the needed products are distributed and point wise run-off both quantitatively and qualitatively. For the offshore boundary condition, 3D current, water quality fields, and wave spectra will be used. For the atmospheric boundary, products from local scale meteorological models (wind, atmospheric pressure and rainfall) are needed. For the seabed, boundary information on sediment composition, bedforms and bathymetry and bio-geo-chemical parameters is essential.

This report addresses the impact assessment for improvements in the four boundary conditions (boundary fluxes from land, free-surface boundary condition, seabed boundary condition and open boundary fluxes) on coastal hydrodynamics and particulate transport. The description of the improved four boundary conditions is followed by examples of concrete impact assessment of the theory into the Catalan coast, Liverpool Bay, German Bight and Gulf of Venice.

1. Overview of the final Field_AC WP3 report

1.1.   Motivation and report objectives

The FIELD_AC project aims at providing an improved operational service for coastal areas and at generating added value for shelf and regional scale predictions. In order to analyze the different process the project has been divided in 6 work packages.

The work package 3 dedicated to boundary fluxesaims to establish and use the best possible boundary conditions for coastal water quality modeling:

- For the land boundary side the needed products are distributed and point wise run-off both quantitatively and qualitatively.
- For the free-surface boundary, products from local scale meteorological models (wind, atmospheric pressure and rainfall) are needed.
- For the seabed, boundary information on sediment composition, bedforms and bathymetry and bio-geo-chemical parameters is essential.
- For the open boundary condition 3D current and water quality fields and wave spectra will be used (from MCS ocean and shelf scale products).

During the FIELD_AC project , two additional delivery reports have been published inside the work package 3:

1. Report D3.1 Methodology (including best practice guidelines) on how to identify and incorporate 'concentrated' and 'distributed' run-off in pre-operational forecasts, based on the input and requirements from our users (Keupers et al., 2011).
2. Report D3.2 Methodology to introduce the 3D boundary condition for river discharges (including practical recommendations) for the 4 studied sites as a function of their prevailing conditions and users needs (Liste et al., 2011).

This Report D3.3 (Final Report, Work Package 3) addresses the impact assessment for the improved four boundary conditions (at boundary fluxes from land, free-surface boundary condition, seabed boundary condition and open boundary fluxes) on coastal hydrodynamics and particulate transport.

1.2.   Report organization

The report is laid out as follows. First a description of the improved four boundary conditions (boundary fluxes from land, free-surface boundary condition, seabed boundary condition and open boundary fluxes) are given. This description is followed by examples of the impact assessment for the improved into the Catalan coast, Liverpool Bay, German Bight and Gulf of Venice). Finally, general discussion and conclusions are given.

2. 'Improved' Boundary Fluxes

2.1.   Introduction

At the scale of coastal waters all boundaries become important. For the land boundary side the needed products are distributed and point wise run-off both quantitatively and qualitatively. For the offshore boundary condition, 3D current, water quality fields, and wave spectra will be used (from MyOcean and/or other shelf scale products). For the atmospheric boundary, products from local scale meteorological models (wind, atmospheric pressure and rainfall) are needed. For the seabed, boundary information on sediment composition, bedforms and bathymetry and bio-geo-chemical parameters is essential. For this reason the boundary fluxes improvement has been:

1. Boundary fluxes from land
2. The free-surface boundary condition
3. The seabed boundary condition
4. Open boundary fluxes

2.2.   Improvements to land boundary condition

The aim here is to incorporate the continental run-off, including both the distributed and point wise (rivers / creeks) run-off for the selected case studies. Numerically these lateral boundary conditions were prescribed to one or multiple model grid points. All available data was interpolated at the exact time step of the model to provide a synchronous continuous source. The main breakthrough was the explicit identification / quantification / qualification of distributed and point-wise run-off in order to quantify the input and budget of sediment and nutrients into coastal waters. Continental/urban run–off is rarely considered in circulation models but can play a crucial role for water quality assessment and prediction on the local scale.

For river outflow, particular attention was paid to incorporating the 3D structure of the discharge (in terms of water / sediment / nutrients). This 3D structure is essential boundary information for a realistic simulation of river plume dynamics and its effect on the "receiving" coastal sea.

2.2.1. Improvements in predicting land boundary fluxes

Report D3.1 entitled "Methodology (including best practice guidelines) on how to identify and incorporate 'concentrated' and 'distributed' run-off in pre-operational forecasts, based on the input and requirements from our users" (Keupers et al., 2011) lists in detail the data needs regarding precipitation, evapotranspiration, digital elevation model, land use, and observations of discharges and water quality. It also explains rigorously how a conceptual model can be set up to predict river runoff (Figure 1) and urban drainage overflow (Figure 2) that can be incorporated into coastal scale oceanographic models.
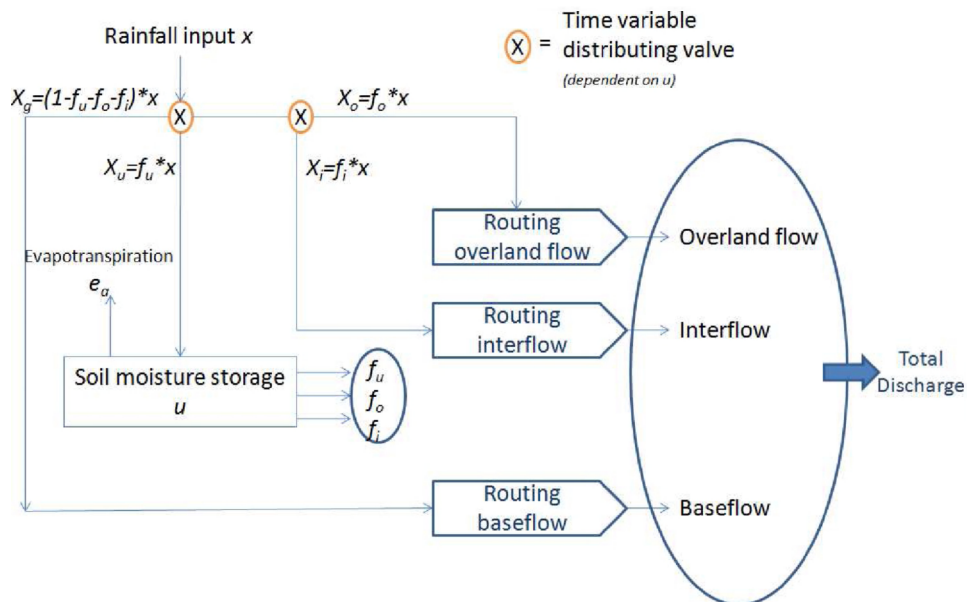
Figure 1. Conceptual river model structure (source: Keupers et al., 2011)
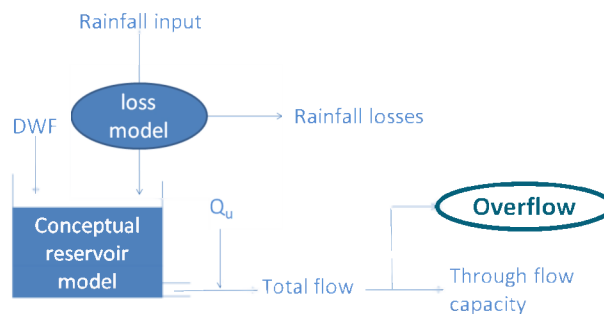
Figure 2. Conceptual CSO model structure (source: Keupers et al., 2011)

For the Catalan coast case study, an executable program has been developed by the KU Leuven that can predict the discharges based on the forecasted rainfall for both the Llobregat river, the Besòs river and the four CSO locations (Ginebra, Bogatell, Bac de Roda and Prim). It has been shown that using conceptual models to predict the freshwater input into oceanographic models is a good approach as reasonably accurate results can be obtained with very short calculation times, an important prerequisite for an operational model.

In contrast to the highly temporally variable Catalan coast region, Liverpool Bay is considered as a second test case. This area is a region of freshwater influence (ROFI) and the Bay is both horizontally and vertically stratified by the inflow from several rivers. As the Bay is highly affected by the presence of freshwater year-round, river climatologies are presently used to take into account the water mass that is generated by rainfall runoff processes on land. However, these time series do not take account the high variation in discharge fluxes that can be seen (Figure 3). On daily and weekly timescales the freshwater forcing is characterised by high intensity and short duration rainfall events. It is unknown how the episodic nature of the freshwater modifies how rapidly the plume mixes in Liverpool Bay. Therefore, the parameters of the conceptual river model have been calibrated for the rivers Clwyd, Elwy, Alyn, Dee, Weaver, Dane, Irwell, Mersey, Ribble, Lune, Kent and Leven. These 12 rivers represent more than 90% of the total freshwater mass flow entering the Liverpool bay area.
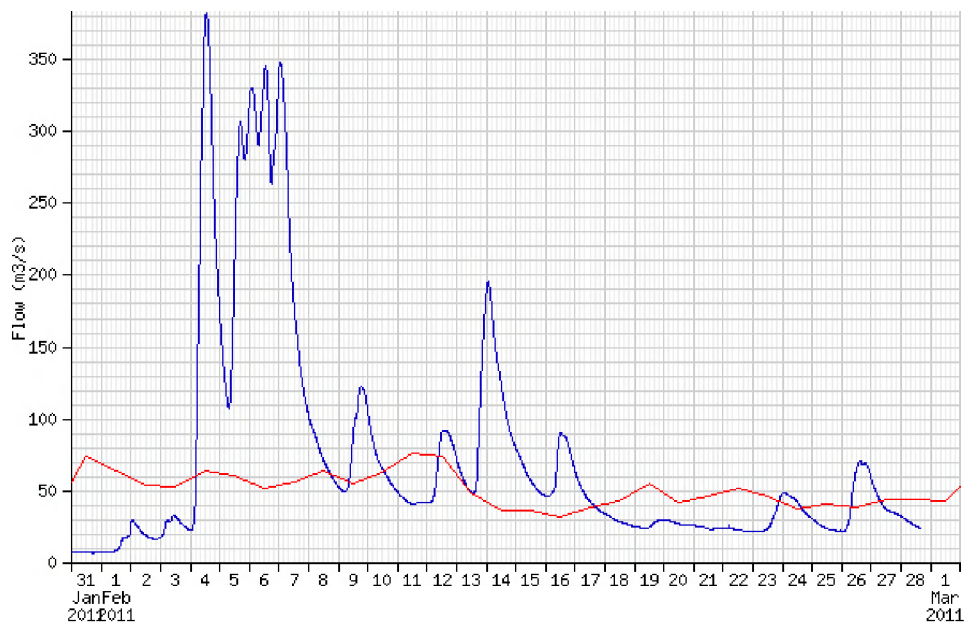
Figure 3. Historical mean (red) and measured (blue) discharge values for the river Ribble

Another issue that has been explored in Liverpool Bay is the effect of the temperature of the incoming freshwater discharge (Polton et al., 2012) on its density and relative buoyancy. In addition to the estuarine flux volume varying throughout the year, the temperature and salinities also vary and both contribute to the buoyancy of the plume. Salinity and temperature are directly measured by an instrumented ferry as it leaves the Mersey for Ireland. There is a clear annual cycle in the temperature field but no annual cycle in salinity as this is determined by episodic rain events. The temperature of the estuary closely matches the air temperature climatology, since the freshwater of the estuary is fed by a network of shallow streams which are efficiently either heated or cooled by the atmosphere. Since the open sea has greater thermal inertia than the atmosphere, the sea temperatures lag the freshwater temperature. In winter the sea is generally warmer than the estuaries, whereas in summer the estuaries are generally warmer than the sea.

The freshwater inflow at the Wadden Sea and Gulf of Venice case study is also considered to be very important and is already included into the oceanographic model as a lateral forcing in the respective hydrodynamic models. Currently, measured or climatological data are being used for this purpose, which is presently sufficient for the pre-operational model that is run. When operational model runs are required in the future, the model structure identification method that is described in report D3.1 can be used to set up the conceptual models that can predict the required discharges in real-time based on forecasted rainfall fields.

2.2.2. Improvements in incorporating the continental runoff into the coastal waters

Through "Work Package 3: Boundary Fluxes" of the Field_AC project, particularly in all issues related to continental runoff into the coastal water (belonging to land boundary fluxes and extensively covered in Report D3.2), the needs to understand and predict the phenomena that control the fate of freshwater after their release in the coastal ocean have been studied. The coastal oceans are the recipient of freshwater and land/drained materials that are primarily brought in through river and urban discharge (Kourafalou et al., 1996). The resulting dynamical structure is called (buoyant) freshwater plume and their proper incorporation as a land boundary fluxes into the sea plays a crucial role for assessment, prediction and management of coastal ecosystems and their resources. In this section of this final report (WP3), the objective is to describe improvements the continental runoff on coastal hydrodynamics.

The main improvements corresponding to continental runoff are detailed below:

- Incorporate the continental runoff into the coastal waters.
- Incorporate combined sewer overflows (CSOs) into the coastal waters.
- Tested different vertical profile structures of the continental discharge.

A 3D hydrodynamical model has been set up to incorporate the continental run-off into the coastal waters. Attention was paid to determine the influence of the discharge with regard to the distributed urban run-off. The 3D structure is essential boundary information for a realistic simulation of river plume dynamics and its effect on the "receiving" coastal waters, for this reason particular attention was also paid to the vertical profile structure of the discharge.

2.3. Improvements to free surface boundary condition

This task has brought in detailed meteorological information - in terms both of wind/pressure fields and rainfall estimates - into the (pre-) operational predictions. Accurate local winds are needed to drive coastal circulation and wave/surge models. For some field cases (e.g. NW Mediterranean) local winds can be particularly important when they come from the land side (imposing for example a tough challenge for wave predictions under short fetches). For the different study sites atmospheric forcing is available either from operational services or from pre-operational high resolution research models.

BSC (Barcelona Supercomputing Centre) contribution:

In order to improve meteorological simulations to provide the meteorological information required by the oceanography modelers, BSC has test several implementations:

- High spatial resolution. The resolution of the meteorological model is a critical point in our application. Oceanography modellers demand high resolution meteorological fields. The skills of meteorological models at high resolution need to be assessed. In this sense, several domains at different horizontal resolution are defined to compare the model results at such resolution.
- Data assimilation of Sea Surface Temperature (SST) from MyOcean. The input variables of the meteorological model are the temperature, pressure, momentum and humidity across the troposphere. Moreover, the sea surface temperature (SST) is an important bottom boundary

condition over the sea. SST assimilation from MyOcean is tested in order to better reproduce local complex mesoscale circulations near the coastal area of Catalonia.

- Physical parameterizations. The meteorological model WRF can be configured with several physical parameterizations. In the sensitivity analysis different physical configurations are used to assess the impact of the physics in the model performance.

- Nesting options; one-way and two-way nest options.

NOCL (National Oceanography Center Liverpool) contribution

The Weather Forecasting and Research model (WRF) has been implemented at 12, 4, and 1.3km resolution for a storm event over the Irish Sea (Bricheno et al. 2012). The outputs were used to force the coupled hydrodynamic and wave model POLCOMS-WAM and the effect on storm surge and waves has been assessed. An improvement was observed in the WRF model pressure and wind speed when moving from 12km to 4km resolution with errors in wind speed decreasing more than 10% on average. When moving from 4km to 1.3km no significant further improvement was observed.
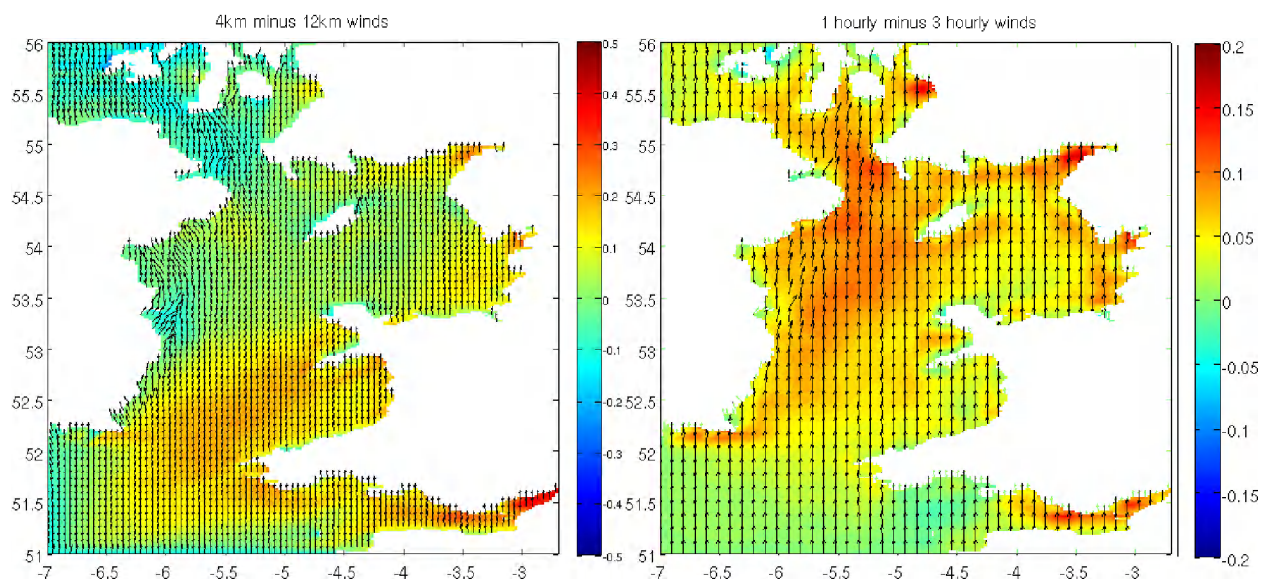
Figure 4. Map of wave height and directional difference in the 1.8km ocean model when comparing 12km and 4km resolution modeled winds (left panel). Map of wave height and directional difference in the 1.8km ocean model when comparing hourly and 3hourly applied 12km resolution modeled winds (right panel) (after Bricheno et al. (2012)).

Sensitivity to frequency of meteorological forcing was tested in this configuration, at 1, 3, 6, and 12 hourly rates. Lower wave heights were found when applying lower frequency wind forcing. Reducing the frequency from 1 to 3 hourly decreases the mean wave height by around 4cm and the

maximum by an average of 13cm. The most extreme differences between using 12 hourly and 1 hourly forcing can be as much as 2m difference in the interior of the Southern Irish Sea. Connected work by O'Neill et al. (2012) investigates model sensitivity of shelf sea surface properties to frequency of meteorological forcing.
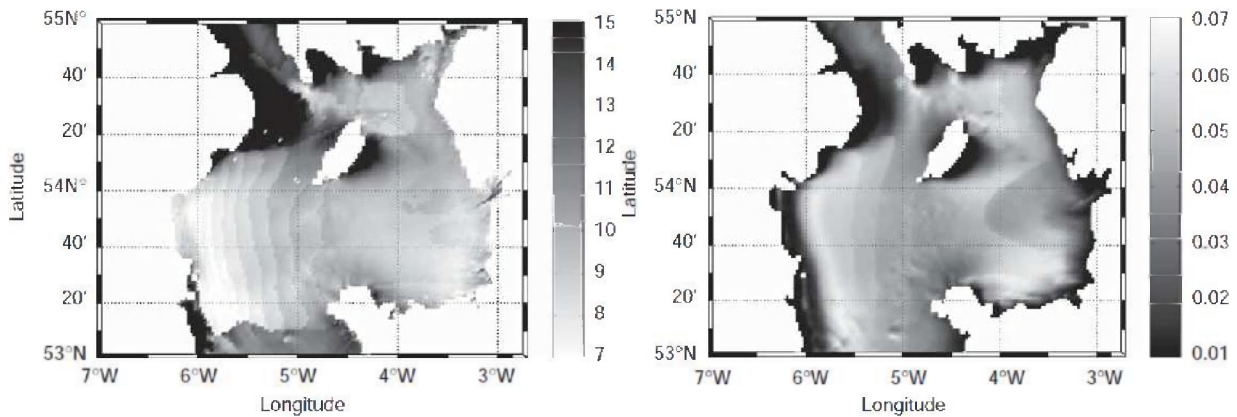
Figure 5. Wave-age at peak surge across the Irish Sea on the 18th January 2007 (left panel). Wave-dependent Charnock parameter at peak surge on the 18th January 2007. With increasing fetch the waves become older, within Liverpool Bay the wave-age decreases due to shoaling (Taylor and Yelland 2001). A steep gradient along the east coast of Ireland is due to the sheltering effect of the land on the wind (right panel) Both after Brown and Wolf (2009).

Brown and Wolf (2009) investigated whether a wave-dependent surface drag is useful for accurate surge prediction, and also if this can be represented by an optimised Charnock parameter. The Proudman Oceanographic Laboratory Coastal Modelling System-Wave Model (POLCOMS-WAM) was used to model combined tides, surges, waves and wave-current interaction in the Irish Sea on a 1.85 km grid.

They concluded that including a wave-dependent Charnock parameter removes the need to find an optimized constant value for different sea areas and model resolution, and will provide an acceptable prediction across the eastern Irish Sea for different surge events. In the medium resolution Irish Sea model, the wave-dependant Charnock value can be represented by a constant Charnock parameter of 0.0185, when considering the regional surge prediction and variations in time. At a given location the maximum surge peak predicted by using the wave-dependent Charnock parameter can be represented by using the larger constant Charnock value of 0.0275.

2.4.   Improvements to sea-bed boundary condition

This task aims at incorporating into pre-operational products the detailed knowledge nowadays available about sediment deposition / suspension near the sea-bed. These mechanisms also apply to pollutants deposited inside and near the entrance of harbours in the studied field cases.

For bed-flow interactions, both the bed composition and its associated bed-forms are important. They play a critical role in flow/sediment coupling and therefore in the resulting fluxes of sediments and pollutants. There is considerable information available for the different project sites, both in terms of bathymetry and bed composition as well as in terms of measurements of SPM fluxes under different forcing conditions.

The work here is, thus, strongly linked to tasks in other work packages: multi-disciplinary database in WP1, sediment transport model in WP2, detailed modelling of interactions between hydrodynamics (waves, currents, turbulence) and sea-bed sediments in WP4 and its application to particular project sites in WP5.

KUL (KU Leuven) contribution:

This section presents a summary of the research contribution of the KU Leuven to the task 2.4, dealing with the bed boundary conditions. This contribution focuses in particular on the bed boundary conditions for the numerical modeling of hydrodynamics and sediment transport. Details of this work are further elaborated in the final report of this task (Toorman and Bi, 2013).

Depending on the complexity of the numerical model, various types of bottom boundary conditions are required for the hydrodynamic equations and (if applicable) sediment transport equations.

Usually, the background and method of implementation of boundary conditions is given little attention in software manuals. Several aspects are not disclosed, making it sometimes difficult to assess certain problems that can be encountered in running a model or understanding the outcome.

Whereas the report provides an overview of current practises, the present summary focuses on a new strategy based on much more physical processes and less on empiricism.

BOTTOM BOUNDARY CONDITIONS FOR HYDRODYNAMIC MODELLING

It is important to realize that all bottom boundary conditions are based on the assumption of local equilibrium. In the case of hydrodynamics, it implies that, at the bed, the streamwise momentum is reduced to the following steady state stress balance:

$$\frac{\partial \tau}{\partial z} = \frac{\partial}{\partial z}\left(\rho(v+v_t)\frac{\partial u}{\partial z}\right) = \frac{\partial p}{\partial x} \tag{1}$$

where: τ = the shear stress, u = the horizontal velocity, p = the pressure, x = the streamwise (i.e. horizontal) coordinate, z = the vertical coordinate (positive upwards and 0 at the bottom), ρ = the bulk density of the fluid or suspension, v = the kinematic viscosity of the suspension and v_t = the eddy viscosity.

Equilibrium implies that the streamwise pressure gradient is constant. Integration of equation (1) over the water depth yields the stress distribution, which is then a linear function of z:

$$\tau(z) = \rho(v+v_t)\frac{\partial U}{\partial z} = \frac{\partial p}{\partial x}(h-z) \tag{2}$$

where: h = the water depth. The bottom shear stress τ_0 is then found to be for (2) at z = 0:

$$\tau_0 = \rho u_*^2 = h\frac{\partial p}{\partial x} \tag{3}$$

where: u_* = the shear velocity (by definition).

Many hydrodynamic models for coastal and estuarine applications are based on the Saint-Venant equations, assuming a hydrostatic pressure distribution. The pressure gradient can then be replaced in terms of the free surface slope (S_h):

$$\tau_0 = \rho u_*^2 = \rho g h\frac{\partial h}{\partial x} = \rho g h S_h \tag{4}$$

2DH hydrodynamic models

In the case of depth-averaged (2DH) models, the interaction of the flow with the bed is governed by the bottom friction closure, which is a sink term in the momentum equation. Usually, a quadratic friction law is implemented:

$$\tau_0 = \rho u_*^2 = \frac{1}{2}\rho C_D |U| U \tag{5}$$

where: U = depth-averaged water velocity, and C_D = the drag coefficient. Various empirical forms (Chézy, Manning, etc.) are commonly used, but apply a friction factor which is often determined by trial-and-error during the calibration phase of the model. The most popular calibration method is the tuning of the friction coefficient resulting is the best agreement of measured and modelled water levels.

However, by assuming the velocity profile to be logarithmic, it is possible to derive a more accurate friction closure. When approximating the vertical velocity profile by the log-law and integrating over the depth yields an expression for the velocity U as a function of water depth and bottom roughness. Substitution in (5) yields the following closure for the drag coefficient:

$$C_D = 2 \left(\frac{\kappa}{\ln(h/z_0) - 1 + z_0/h} \right)^2 \quad (6)$$

where z_0 = a roughness length scale (see below).

Physical roughness

Physical roughness is generated by unevenness of the bottom. One can distinguish three levels, from small to large: the grain roughness, the bed form roughness and the topographic roughness.

The length scale of these roughness elements is smaller than the horizontal distance between neighbouring grid nodes in meshes for typical coastal and estuarine applications. Moreover, the bottom surface between two adjacent nodes is approximated as being flat, i.e. a linear interpolation of the bottom levels between grid points, which does not capture the actual shape. Therefore, the corresponding subgrid scale effects of the actual surface on the hydrodynamics are included in the roughness closure.

The roughness height z_0 is usually related to the equivalent Nikuradse roughness by:

$$z_0 = \frac{k_s}{30} \quad (7)$$

A ripple predictor may be useful in the case of non-cohesive sediments. Furthermore, one can also work with a bottom composition dependent value of k_s.

Drag modulation by suspended sediment

Besides the physical roughness, experimental data show drag modulation depending on the sediment concentration. Two observations are made:

1) The slope of the log-law, i.e. the inverse of the von Karman coefficient, changes. Laboratory and numerical experiments indicate that the von Karman coefficient changes from its clear water value $\kappa_0 = 0.41$ to (Toorman, 2002):

$$\kappa = Sc \frac{w_s}{u_*} \quad (8)$$

with w_s = the settling velocity, Sc = the turbulent Schmidt number. A value of Sc = 0.7 seems a good value (Toorman, 2011). However, the relationship between the actual value of κ and concentration field has not yet been established, in particular for cohesive sediments, for lack of experimental data.

2) The velocity decreases with increasing sediment load. Analysis of the flume experiments with sand of Cellino (1998) with a new Generalized Mixing-length (GML) theory (Toorman, 2013) suggest that the corresponding apparent increase in roughness is proportional to the concentration. This roughness increase is physically explained by the energy loss due to 4-way interactions between particles and turbulence (Elghobashi, 1994). In terms of the GML theory, it actually represents subgrid-scale turbulence generated in the wake of the particles. Therefore, the empirically found proportionality with concentration is in agreement with these theory-based expectations.

However, in the case of cohesive sediments, instead of increasing drag, drag reduction due to high suspended loads is observed (Wang *et al.*, 1998; Li & Gust, 2000). This suggests that the first mechanism remains dominant. Most likely, high-concentrations of mud flocs occupy too much space to allow turbulence production in the wake and are more easily moved with the surrounding water due to lower inertia.

Low-Reynolds drag law

Equation (6) guarantees that C_D becomes infinite when the water depth reaches the roughness height. Therefore, it has the additional advantage that the threshold for drying-flooding schemes can now be reduced to much lower values (with a minimum of z_0) than traditionally taken.

However, not all the numerical problems are removed by this closure. Implementation of (6) in a code (Open Télémac v6 in our case) shows that the dependence of the drag on water depth may still cause numerical problems when the water level becomes small. The explanation is that in reality, one has to account for the fact that in the limit the flow becomes laminar. This is of importance in the first place for the intertidal flats.

Therefore, the drag closure has to be modified to ensure that its value asymptotically goes to the laminar drag solution:

$$\sqrt{\frac{C_D}{2}} = \frac{u_*}{U} = \sqrt{\frac{2\nu}{hU}} \qquad (9)$$

However, in the case of a rough bottom the laminar stress has to be modified in order to account for the turbulence dissipation due to vortex separation between roughness elements. Since the velocity log-law is no longer valid in this layer, the velocity profile is computed from a new Generalized Mixing-length model, which extends the traditional Prandtl mixing-length theory down to the bed, i.e. it covers the inner boundary layer (comprising the viscous sublayer and the transient layer) and accounts both for rough bottom surfaces and suspended sediments (Toorman, 2013).

In order to allow both transient (between turbulent and laminar) conditions (i.e. $5 < h_+ \ (= hu_*/v) < 100$) and the transition during drying/wetting of tidal flats, it is necessary to combine the laminar and turbulent contributions. This is obtained by superposition of the laminar and the turbulent stress, where the turbulent stress is damped towards the bottom (conform observations, and simultaneously avoiding numerical problems).

Hence, the computation of u_* is then written as the following superposition of the laminar and the turbulent contributions:

$$u_*^2 = f_A u_{*turb}^2 + u_{*lam}^2 \tag{10}$$

with f_A an empirical (quadratic exponential) damping function, as apperaring in the low-Reynolds mixing-length model (the GML model).

<u>Suspension flow case</u>

Analysis of the experimental data of Cellino (1998) shows that the corresponding roughness modulation is proportional to the local concentration (Figure 6).

For the 2DH application, the shear velocity in the most general case is then obtained by replacing z_0 by $(z_0 + \beta ch)$ in the "laminar" contribution and the final form of the shear velocity is given by (Toorman & Bi, 2013):

$$u_*^2 = f_A \left(\frac{\kappa U}{\ln(h/z_0) - 1 + z_0/h} \right)^2 + \left(\sqrt{\left((z_0 + \beta ch) \frac{U}{h} \right)^2 + 2 \frac{U}{h} v} - (z_0 + \beta ch) \frac{U}{h} \right)^2 \tag{11}$$

where c = the depth-averaged (volumetric) sediment concentration. The water depth h is included in the apparent suspension roughness to make the formula consistent in terms of units. β is the suspension friction coefficient, see below.

The generalized bed roughness (which actual form needs to be confirmed by further research) thus requires only two calibration parameters, of which z_0 is directly related to the Nikuradse roughness (i.e. the physical roughness height k_s), while the suspension roughness coefficient β has to be found (for the time being) by trial and error (i.e. a model tuning parameter).

Finally, there is also a third parameter (A_+) appearing in the damping function. It is expected that its value (18 by default, calibrated with DNS data for clear water over a smooth surface) will have little influence on the large-scale flow, but this needs to be confirmed by future work.
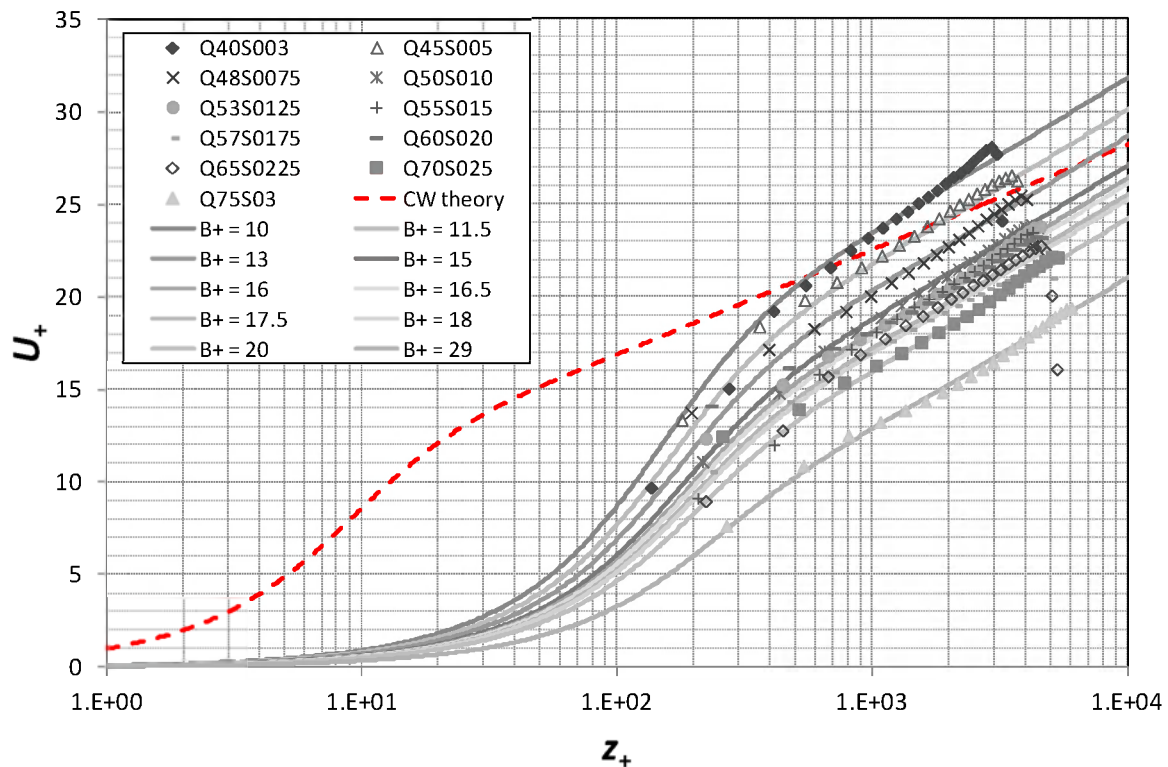
Figure 6. Comparison of non-dimensional velocity profiles by the Generalized Mixing-Length model with flume data of CELLINO (1998) for sand suspension flow with increasing sediment load. Symbols = measurements, full lines = calculations, dashed line = velocity profile for clear water, B+ = GML model parameter, proportional to the sediment concentration. (U+ = U/u* = velocity U non-dimensionalized by the shear velocity u*; z+ = zu*/ν = distance from the bottom z non-dimensionalized by the length-scale ν/u*, where ν = the kinematic viscosity of the ambient water). CW = clear water.

Application test case: Western Scheldt sediment budget

The new friction law has been implemented into the Open Télémac software[1], applied to the Scheldt Estuary (Belgium and the Netherlands) (Figure 7), within the framework of the FP7 Theseus Project[2]. In order to objectively compare the model outcome for a traditional approach with constant Chézy number and the new friction law, the sea boundary has been forced with a simple bi-harmonic tide imposing the water level as a function of time (Figure 8). At the downstream boundary a constant fresh water discharge (of 200 m³/s) has been imposed. For the sediment transport equilibrium profiles are imposed on all open boundaries.
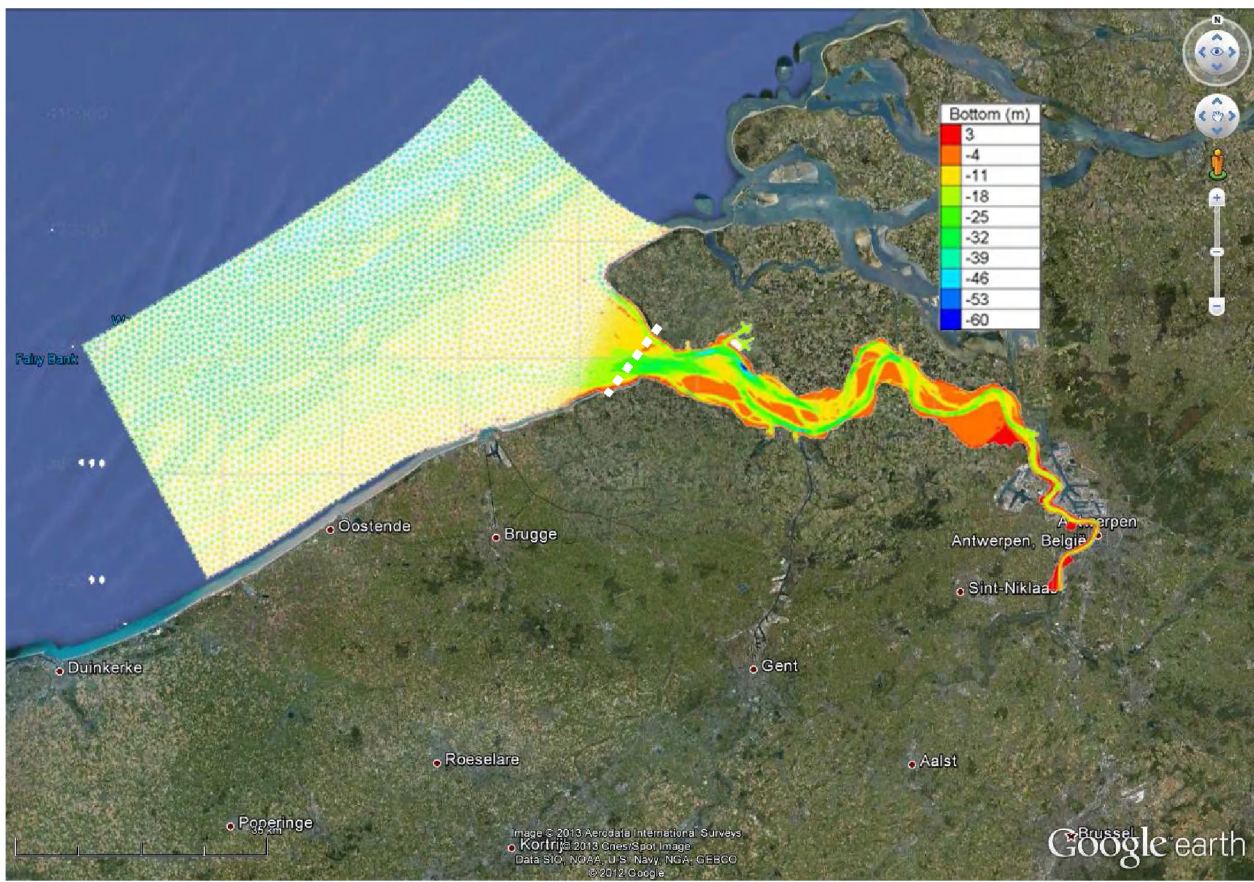
Figure 7. Scheldt-Belgian Coast model domain, mesh and bathymetry.

Dotted (white) line = cross section for flux calculation.

---

[1] www.opentelemac.com

[2] www.theseusproject.eu
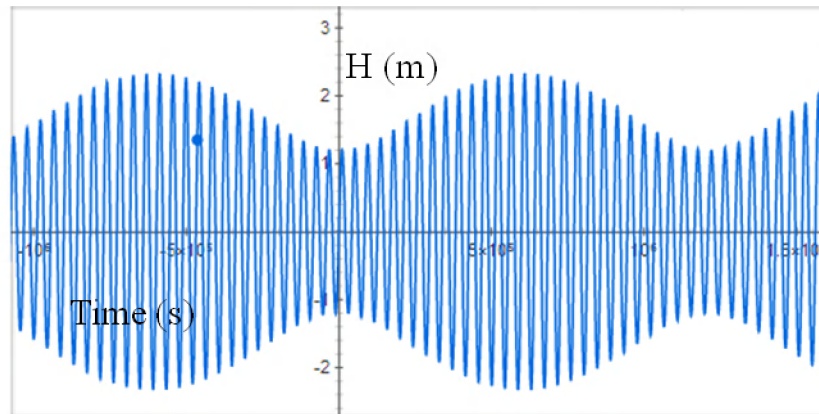
Figure 8. Bi-harmonic tidal forcing used as sea boundary condition for the Scheldt model.

The first variant of the model runs for cohesive sediments, while the new bed roughness model applies values for sand, derived from the Celino flume experiments (at present the only available data to calibrate the new friction law). This is not entirely consistent. Nevertheless, since sand transport also occurs, while the mud concentrations are used, it is not completely illogic that the apparent bed roughness is dominated by sand (mainly transported as bed load) rather than by mud.

The model has been calibrated for the hydrodynamics for the water levels. No true calibration for the sediment transport parameters was carried out at this stage, but a rough calibration was performed in order to obtain SPM concentrations of the same magnitude as measured in the field. The following conclusions could be drawn from the results:

- Without invoking sediment transport, the results for the hydrodynamics between the traditional and the new friction law are minimal. But the new friction law allows to reduce the threshold for inundation to the bed roughness height, without generating excessive velocities.
- Once sediment transport is switched on, the results for hydrodynamics change a bit in the sense that the flow experiences more bottom friction, resulting in a slightly lower tidal intrusion. Hence the amplitude of the tide reduces slightly throughout the estuary upstream.
- The patterns of SPM concentration in various points now clearly show differences. When the same settling velocity is used for both cases, the new friction law produces lower SPM concentrations because the increased friction implies more energy dissipation in turbulent eddies and less energy available for suspending particles.
- In order to evaluate potential effects on long term sediment transport, the settling velocity in the constant Chézy case was reduced by a factor 2, such that the same SPM concentrations in the Wester Scheldt mouth area are obtained as with the new friction law. Subsequently, the net sediment budget over a one month period was calculated for a cross at the mouth (roughly between Vlissingen at the north shore and Cadzand at the south shore –). The outcome shows that the new friction law generates significantly lower net transport (about 3 times in this case) than the constant Chézy case (Figure 9). The settling velocity does not really affect the long-term flux (Figure 9).

The second variant of the model employs the mixture model approach, adapted from Waeles *et al.* (2007). Since the bed contains much less cohesive material than in variant 1 (entire bed cohesive), the total amounts of suspended matter is significantly lower, which results in (more than one order of magnitude) lower sediment fluxes (Figure 10), closer to estimates based on field data. The longer simulation shows that the sediment flux varies stepwise over each spring-neap cycle (Figure 10). The new friction law again predicts about 3 times lower sediment fluxes.
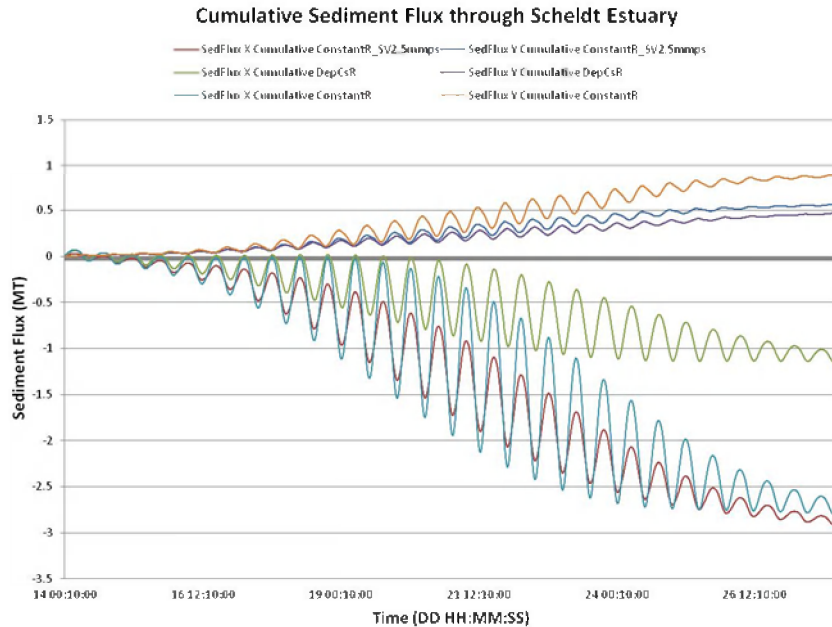
Figure 9. Evolution of the cumulative net sediment flux (in x = east and y = north directions) over one spring-neap cycle for the 1st model variant with entirely cohesive sediment bed.
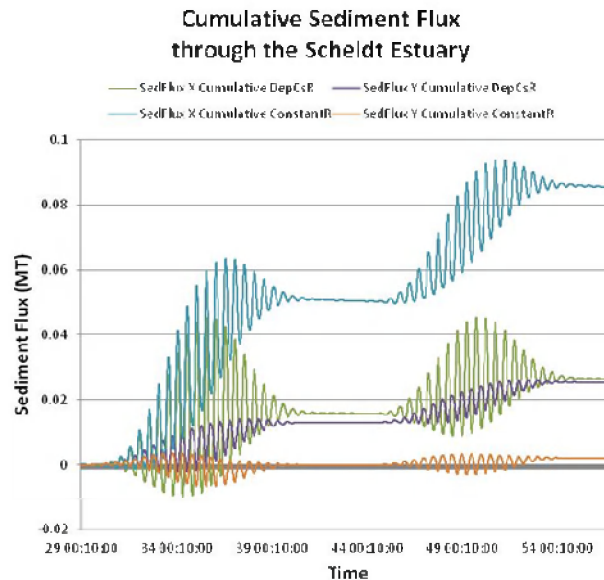
Figure 10. Evolution of the cumulative net sediment flux (in x = east and y = north directions) over two spring-neap cycles for the 2nd model variant with mixed sediments.
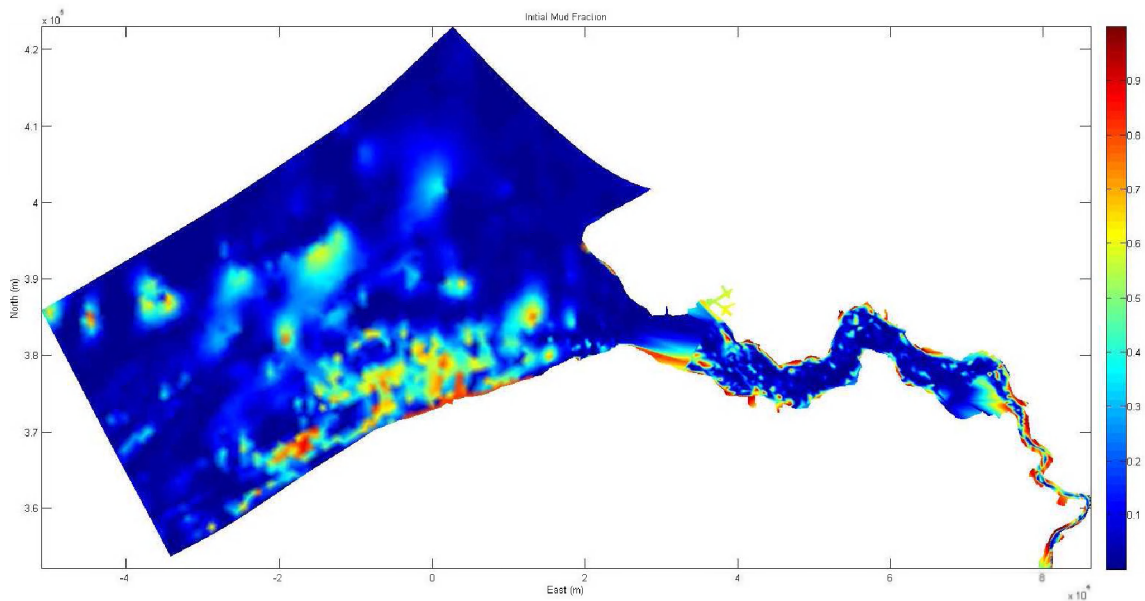
Figure 11. Distribution of the mud fraction of the sediment bottom (data provided by Flanders Hydraulics, Flemish Ministry of Public Works, for the estuarine part and BMM, Royal Belgian Institute of Natural Sciences, for the coastal part).

It is interesting to notice that the direction of the net sediment flux is opposite for the two model variants, showing once more the high sensitivity of sediment transport model predictions to the model settings.

The model results also show that the mud fraction distribution (Figure 11) does not vary much over a spring-neap cycle.

Since this is the first real application test of the mixture model in Télémac, the presented (uncalibrated) results should still be considered with care as preliminary and need further investigation, as well as calibration against field data.

A more in depth analysis of the various model variants and parameter settings is discussed in the report (Toorman & Bi, 2013).

The major conclusion is that both model variants confirm the hypothesis that the effect of high SPM concentrations above the bed has significant effects on the estimation of sediment budgets. ***This is of vital importance for authorities managing ports and waterways, to make proper estimates of e.g. maintenance dredging costs or sand balances for beach morphodynamics.***

3D hydrodynamic models

In the case of 3D models, the bottom friction law is now used to determine the shear velocity, which is used in the formulation of the near-bottom-boundary conditions for the velocity and (if applicable) the *k*-epsilon turbulence closure model.

The boundary conditions for hydrodynamics (velocity and turbulence) usually are imposed in a node above the bottom where turbulence is fully-developed. This avoids the computational expensive need to resolve the flow in the laminar and transient boundary layer above the bed.

Moreover, this layer is usually thinner than the roughness heights of the bed forms, which are not resolved, since their length scales are smaller than the horizontal grid spacing. Therefore, bottom roughness and the bed boundary layer have to be dealt with as subgrid-scale levels.

Few software manuals actually describe clearly the way that bottom boundary conditions are implemented. In theory, the true distance of the bottom node relative to the true bottom needs to be specified, but this information usually is lacking.

For the hydrodynamics, the bottom boundary condition is often the bed shear stress itself (i.e. the velocity gradient) as a natural (or Neumann) condition. This requires at least one non-zero reference velocity being imposed somewhere else in the domain, usually at an open boundary (e.g. a river discharge).

Alternatively, one can also impose the velocity in the near-bed node, assuming a velocity profile (usually the logarithmic velocity law, following the Prandtl mixing-length theory). The latter method has proven to result in a more stable convergence behaviour (at least in the KU Leuven FENST-2D research code).

Full details of the traditional boundary condition procedures are listed in the report, including the adaptation to 3D of the new strategy described above for 2DH (Toorman, 2012). Within the framework of FIELD_AC the full 3D version could not be tested because the 3D sediment transport module of the Open Télémac software was not available until the release of version 6.2. The release in August 2012 was too late to be tested within this project.

BOTTOM BOUNDARY CONDITIONS FOR SEDIMENT TRANSPORT MODELLING

No new boundaries for the sediment transport equations have been derived within the framework of FIELD_AC. Nevertheless, since little attention is given to the detailed description of the procedures

and justification of sediment boundary conditions, the full details are found in the report (Toorman, 2012). A summary is given here.

2DH sediment transport models

For the sediment transport, the exchange with the bottom is governed by erosion and deposition criteria, appearing respectively as a source and a sink term in the SPM transport equations.

Based on suspension capacity theory, Toorman (2013) has demonstrated that the critical stress for deposition (τ_D) in the popular deposition law of Krone (1962) for cohesive sediments, which multiplies the potential deposition flux $w_s C$ (where w_s = the particle settling velocity, and C the depth-averaged SPM concentration), with a probability p_D:

$$p_D = \max\left(0, 1 - \frac{\tau_0}{\tau_D}\right) \qquad (12)$$

can be expressed in terms of the suspension capacity of the flow. This reduces the empiricism in this closure.

Some codes impose the actual bottom deposition flux by computing the near-bottom reference from the depth-averaged concentration using a Rouse profile.

3D sediment transport models

In 3D modelling, sediment concentrations are computed over the vertical allowing the prediction of vertical profiles of SPM. Because of the problem of the subgrid scale of the viscous and transient boundary layer, it is impossible to model the profile correctly to the bed. Two approaches are encountered.

In the first approach, primarily applied to cohesive sediments, only suspension transport is considered. The bottom boundary condition for the sediment transport equation is now a flux boundary condition (Neumann condition), consisting of the sum of the deposition flux (the product of the near-bottom values of settling velocity and concentration) and the erosion flux. This usually underestimates the sediment concentration at the bed, because the shape of the concentration profile cannot be matched with the simple first (or rarely) second order interpolation function, used to connect the concentration values in the nodes where the equations are solved.

Moreover, since most of the models do not resolve the low-Reynolds layer, and start in the log-layer, the alternative is to impose the concentration is this near-bottom node. Various empirical predictors proposed in the literature can be used.

It should be noticed that some models still apply the Krone deposition law with a critical stress for deposition in 3D mode, however using the bottom SPM value instead of the depth-averaged value.

In the second approach, primarily applied to non-cohesive sediments, either an empirical bed-load transport formula is applied, in combination with erosion-deposition criteria, or bed load transport is combined with suspended load transport. The reference concentration at the interface between bed load layer and suspended load layer is again determined by a semi-empirical formula and used as near-bottom boundary condition for the suspended load.

With the new modelling strategy where the low-Reynolds layer is explicitly computed using the GML theory, the sought-after reference concentration in the near-bottom node is computed by numerical integration of the transport in the low-Reynolds layer. Again, it is preferred to explicitly impose this concentration as an essential (Dirichlet) boundary condition, since the interpolation functions are not adequate enough to approximate the true concentration profile over the low-Reynolds layer.

UPC Contribution:

In regional scales solve the gradients in velocity and the bottom boundary layer is difficult. In this sense the Catalan Sea application developed by LIM/UPC have used multiple algorithms to solve de Bottom Boundary Layer (BBL). Using the COAWST (Warner et al., 2010) system, that consists in a methodology to solve the coupling between ROMS and SWAN and in consequence the wave effect on currents, complex formulations has been used. These formulations are based in BBL models that consider both effects: wave and current action on bottom shear stress (e.g.: Styles and Glenn, 2000; Soulsby, 1995; Blaas et al., 2005; Warner et al, 2008). These complex routines simulate BBL processes in the presence of waves and mobile sediment. The short (order-10 s) oscillatory shear of wave-induced motions in a thin wave-boundary layer produces turbulence and generates large instantaneous shear stress (Warner et al., 2008). As example, nested coupled-models in Catalan coast have allowed to determine spatially the prevalent processes in the region: wave-

dominated or current-dominated bed. In Figure 12, the current, wave and current+wave are shown in function of the wave height. The figure show how the wave dominates in a region near the shoreline. In opposite, the current-stress prevails in the river discharge region and offshore.
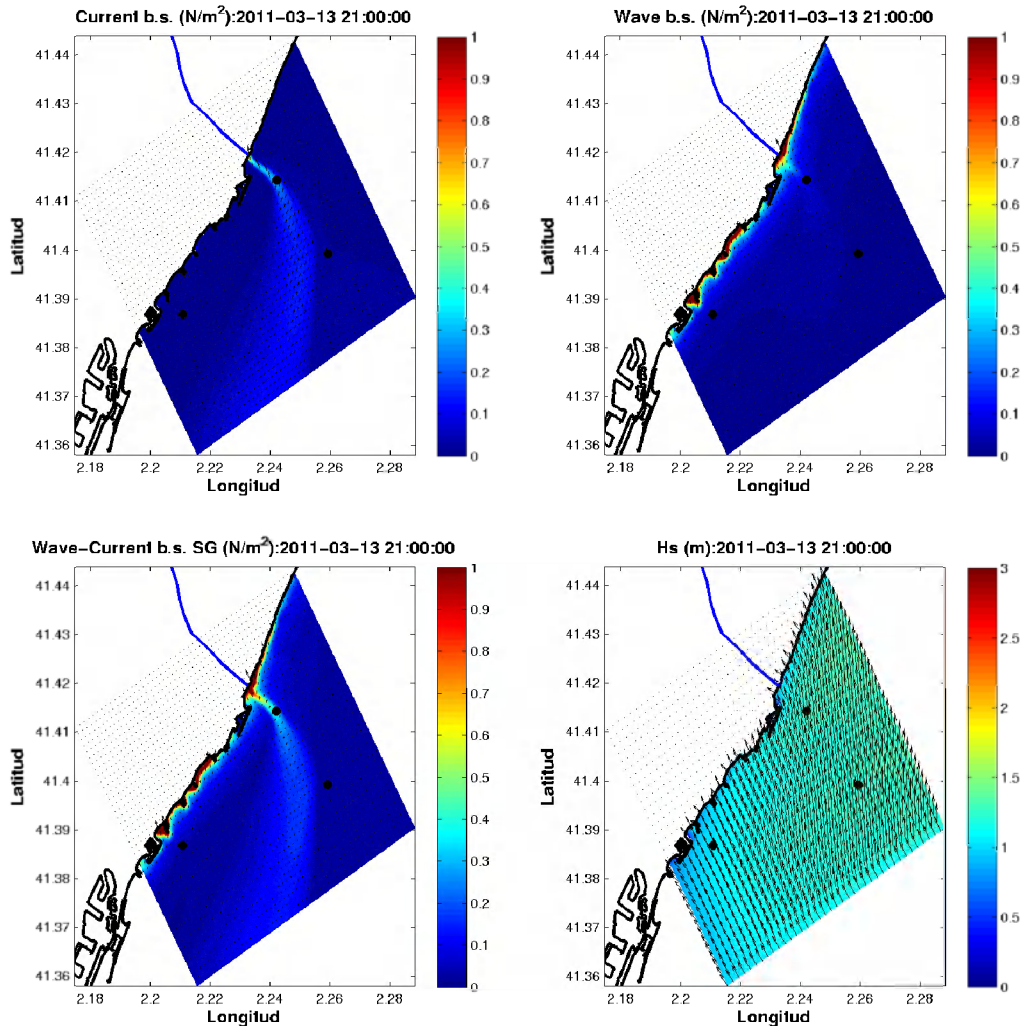
Figure 12. Snapshot of current-stresses, wave-stresses, wave+current stresses and wave height for a high water discharge from the Besòs river.

HZG Contribution

The experiments studying the response of the German Bight circulation to the different bottom roughness are described below. The German Bight model is run for 2 months starting from the 01.10.2011 with the same initial conditions taken from the main experiment (Table 1). As a default in our German Bight model we use a homogenous bottom roughness from 0.01 m (Exp.1). We performed several sensitivity experiments, in which the bottom roughness has been decreased 10

times (Exp.2), increased two times (Exp.3) or even using a space variable bottom roughness (Exp. 4). The time mean difference of the bottom salinity between the experiments is shown on Figure 13. It can be clearly seen that the differences in the bottom salinity are more pronounced in the coastal areas of the German Bight, especially in the front of Elbe and Wesser and Ems rivers. Offshore deeper area is not much sensitive to the bottom roughness.

	Z0
Experiment 1	0.01Realistic
Experiment 2	0.001
Experiment 3	0.02
Experiment 4	Special variability (min=0.005-max=0.017)

Table 1. Table of the experiments with different bottom roughness
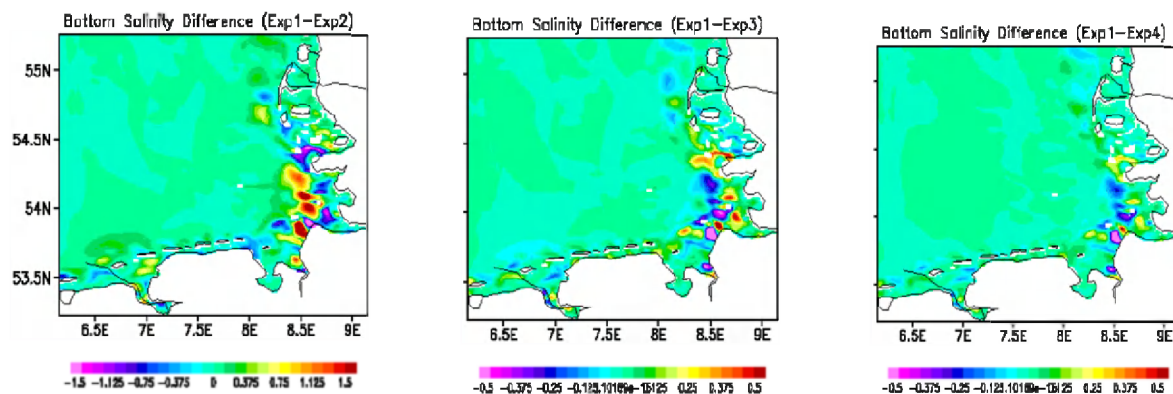
Figure 13. Bottom salinity difference (psu) averaged for October and November 2011 between the sensitivity experiments to the bottom roughness, as described in the Table.

SHOM Contribution

In intermediate to shallow water (shallower than the surface wave length) the orbital velocities of the surface gravity waves extend down to the sea floor which causes an interaction between the waves and the bottom. Shemdin et al. (1978) established an inventory of all the processes of interaction between the wind wave and the bottom. The influence of the bottom manifests itself through a modification or a dissipation of the wind wave. On the one hand, the geometry of the bottom boundary refracts, reflects and scatters the waves. On the other hand, other mechanisms due to the nature of the sea bed, but this time in terms of a damping effect, are also well known such as the motion of sediment, the percolation in a permeable bed, the absorption of energy by the

lutocline (near bottom fluid mud layers) and the bottom friction. The knowledge about bottom friction under waves is required to understand various phenomena related to wave modification and sediment movement. Many processes are present in the evolution of waves in shallow waters, analysing of the energy balance by separating all these processes is a difficult task but it has been shown that the energy balance has needed a dissipation by bottom friction in shallow water to be complete. Recording dissipation by bottom friction is feasible outside the surf zone, in the absence of wind, strong currents, and over a distance short enough to not intercept a significant non linear transfer across the spectrum. The dissipation by bottom friction is one of the processes of wave and bottom interaction the is most studied in wind wave modelling. There is a large literature on bottom friction dissipation under oscillatory waves.

The majority of the authors developed models for monochromatic waves from laboratories studies using water tunnels or oscillatory trays. Two types of models have arisen from the laboratory experiment, one is based on a drag force and the other one on the eddy-viscosity.

The model the most widely used is the formulation of JONSWAP, this drag law model is based on an empirical constant that is used for the dissipation of the entire wave spectrum. The recommended values of JONWSAP constant are in the range of 0.038 to 0.067 (Hassemann & Collins, 1973; Bouws & Komen, 1983). The JONSWAP parameterization for bottom dissipation ignores totally the nature of the bottom and especially the roughness (**Kn**) which has been shown to be one the predominant characteristic of the soil that influences the dissipation by friction, after the depth (Tolman, 1995).

In order to access to the importance of the seabed boundary layer in a spectral wave model in the inner shelf, the model JONSWAP has been compared to the model used by Ardhuin et al. (2001). The parameterization (hereafter indicated as **BT4**) of the interaction of waves with a sandy bottom including ripples generation and relict ripple roughness (Ardhuin et al. 2003) using the sub-grid roughness algorithm by Tolman (1995). It allows fractional ripple coverage for the grid box considered, modified to take a better account of the relic roughness and extended to take into account the variability of the bottom nature. This model is based on the ripple roughness predictor from Grant and Madsen (1982), elaborated from laboratory data, extended to spectral waves (Madsen et al. 1988) within the sheet flow regime, based on the model of Wilson (1989), is representative for irregular waves. Hence, the bottom friction source term is expressed as follows:

$$Sb_{fric} = -f_w u_b F \frac{(2 \Pi f)^2}{2g} \sinh^2(kd)$$

(13)

$$f_w = \frac{0.08}{Ker^2(2\sqrt{\varsigma_0}) + Kei^2(2\sqrt{\varsigma_0})}$$

(14)

$$\varsigma_0 = \frac{1}{21.2K} \sqrt{f_w} \frac{k_N}{a_r}$$

(15)

$$u_r = \left(2 \frac{(2 \Pi f)^2}{\sinh^2 kd} F\right)^{1/2} , a_r = \left(\frac{2}{\sinh^2 kd} F\right)^{1/2}$$

(16)

Where F is a two dimensional spectrum, d is the depth, f_w is the wave friction factor, K is the Von Karman constant and *Ker* and *Kei* are Kelvin functions of zeroth order, a_r and u_r are a representative near-bottom orbital amplitude and velocity. when the wave energy is distributed over a range of frequencies. Madsen (1994) demonstrated that a representative wave can be used to evaluate the wave boundary layer, consequently, a single bottom roughness and friction factor are used to dissipite the entire wave spectrum (Trowbridge and Agrawal, 1995; Beach and Sternberg, 1992 ; Madsen and Wikramanayake, 1991).

The equivalent roughness **Kn** (Nikuradse equivalent bottom roughness) is, in the sediment transport community, a combination of the skin friction, the bedform (in the case of sandy bottom, waves and currents may generate bedforms) and also the apparent roughness due to a thin layer of highly concentrate sediment saltating and suspending at the bottom. In the wave modelling community, Grant and Madsen defined the Kn as the sum of a ripple roughness k_r and the sheet-flow roughness k_s. Tolman (1993) defined the sheet flow roughness as an apparent roughness due to a thin layer of highly concentrated, saltating and suspended sediment. When ripples are not generated, the roughness Kn0 is related to the sand grain size, and to the historic of previous hydrodynamic conditions (currents and waves). This minimum roughness is fixed at 0.01m by Tolman (1994), it is corresponding to the relic roughness, current-induced roughness and bioturbation. Ardhuin et al.(2003) found that the constant value proposed by Tolman (1994) of 0.01m does not appear to be adequate and on the comparisons between observed and modelled-predicted significant attenuation of long period swell over relic ripples he concluded that the roughness should depend on the wave orbital excursion. So the main difference between both communities in the definition of the roughness is that the wave modeller would prefer to separate the different regimes (active ripples or no active ripples) and the skin friction would be deleted in case of actives ripples.

Kajiura (1968) reported that Bagnold (1946) was the first to give an empirical formula of the friction coefficient of the quadratic friction law for an oscillatory flow in the presence of artificial ripples. Tolman (1994) is probably the first one to implement and investigate a movable beds friction model for bottom friction dissipation in a spectral wave model. Bagnold (1946) found that the friction coefficient decreases with the increase of the amplitude of wave bottom orbitals velocities. Tolman (1994) has described three distinct regimes (Figure 14) that function of the increase of the wave velocities orbital: "the no-ripples formation regime" in which the friction factor decrease slowly, "the ripples formation regime" that perform a sharp increase of the friction factor at the initiation of ripples followed by a decrease and "the sheet flow regime" that evolves with the increase of the friction coefficient.
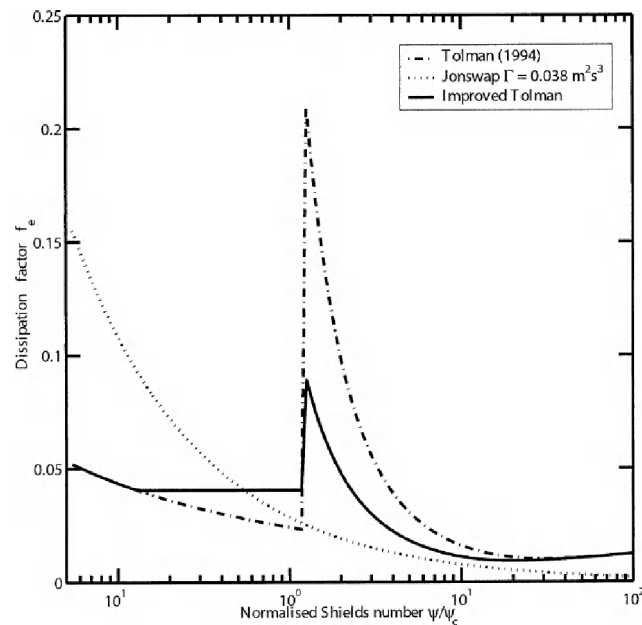
Figure 14. Dissipation factors f_e as a function of the Shields number c normalized by its critical value c_c for sediment motion. The original parameterization proposed by Tolman (1994) based on the Madsen et al. (1990) laboratory experiments is compared with a slightly modified formulation tuned to the field data (see Part I) and the widely used JONSWAP parameterization.

On noncohesive sandy bottom, the ability of the near bed wave orbital motion on sediment to create ripples are governed by the normalized Shields number $\Psi_N = \psi / \psi_c$ (ratio of friction $f_{w,s}(Kn = D50)$ and buyant forces acting on a median sand grain D_{50} and its critical value for initial motion so called the critical Shield number).

$$\psi = f_{w,s} \frac{u_b^2}{\left[g(s-1)D_{50} \right]} \tag{17}$$

$$\psi_c = \frac{0.3}{1+1.2 D_{star}} + 0.055 \left[1 - \exp(-0.02 D_{star}) \right] \tag{18}$$

$$D_{star} = D_{50} \left[\frac{g(s-1)}{v^2} \right]^{1/3} \tag{19}$$

$$\frac{k_r}{a_r} = 1.5 \left(\frac{\psi}{\psi_c} \right)^{-2.5} \tag{20}$$

$$\frac{k_s}{a_r} = 0.0655 \left(\frac{u_r^2}{(s-1) g a_r} \right)^{1.4} \tag{21}$$

$$\frac{k_{N0}}{a_r} = max(0.01 m, 0.05 a_r, \eta D_{50}) \tag{22}$$

For value of the normalized Shield number less than 1.2 (determined in laboratory experiments with random waves Madsen et al. 1990), no sediment motion occurs thus the Kn retained is the relic roughness. Past the threshold of 1.2, the wave flow intermittently moves surficial sediments that organize into ripple fields (Nielson 1981; Trayvoski et al 1999).

Both bottom friction parameterizations (JONSWAP + BT4) have been used to realize a hindcast on the year 2003 with the help of the spectral wave model WAVEWATCH III. The description of the model has been fully described in the D2.2 with respect of all the parameters and sources terms used. We used the global database on sediment mapping of the SHOM (Garlan et al. 1993) to introduce the median grain size in the model grid with the BT4 parameterization. We used the comparison of the result with the field campaign EPEL realized and funding by the SHOM in 2003 that has been presented to the EGU meeting in April 2012. Both models furnished results in agreement with the data and it was clearly not possible do distinguish which parametrization obtained better results. This has been explained mainly by the fact that the bottom nature was equal along the transect, and the coarse sediment present didn't formed any ripples during the campaign. So this field campaign EPEL was useful for validating the skin friction of the model BT4 but unfortunately not for the moveable bed model. In order to extend the validation to the entire area of interest, we used the satellite data. The global validation of the year 2003 is quite similar regardless the parameterization chosen. However, the BT4 parameterization has permit to obtain sensibly better results in the North Sea especially along the French and Belgian coasts.
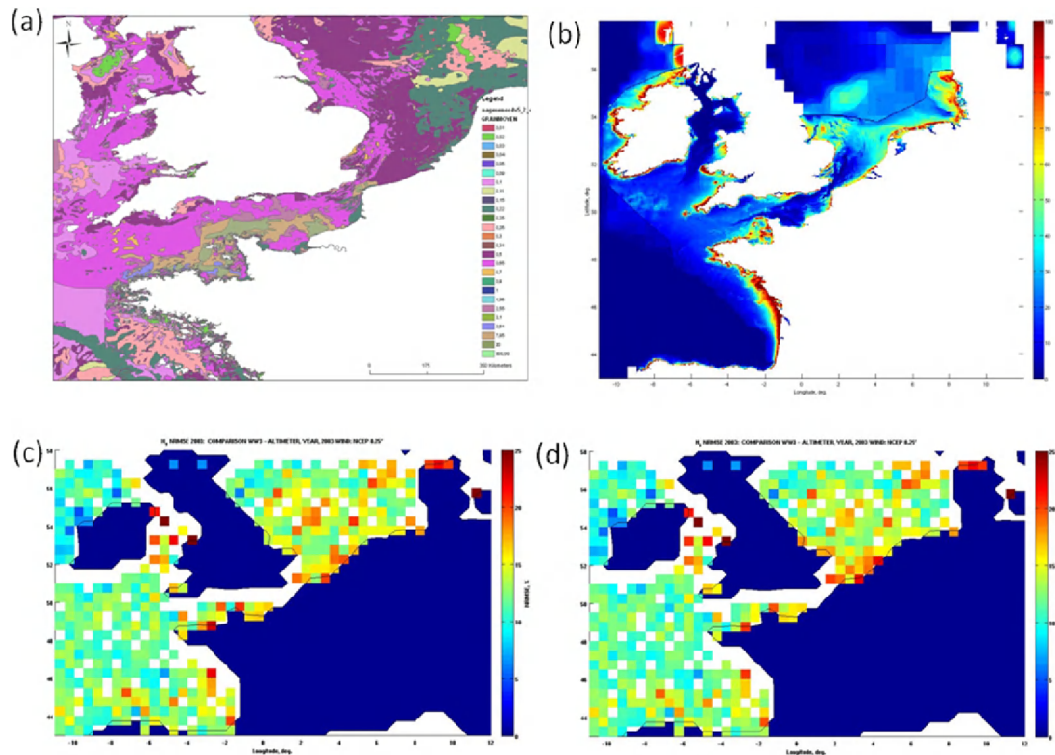
Figure 15. (a) The SHOM global database on sediment cover. (b) Occurrence of dissipation by botton friction (%). (c) Comparison of model result using BT4 and altimeters data during 2003 (NRMSE %).(d) Comparison of model result using JONSWAP and altimeters data during 2003 (NRMSE%).

The occurrence of dissipation by bottom friction (Figure 15 panel b) during one year in the inner shelf is reaching the value of 20%. In the German Bight, the occurrence is higher, but this can be explained by shallow environment rather than the occurrence of long swells periods. To access to the real improvement of the model a selection of the altimeters data should be done with as criterion dissipation by bottom friction of the models superior to zero.

To conclude, an update version of the moveable bottom friction of Tolman (1994) has been implanted and tested. The validation with altimeter data and buoys has shown a small improvement of the results in the North Sea along the French and the Belgian coast. The model BT4 needs some improvement to clearly demonstrate its efficiency on a heterogenic bottom and mobile sediment which is not taken into account in the JONSWAP parameterization. The relative success of a constant value of a content drag coefficient, which does not have a sound justification, (JONSWAP model) may be explained by the fact that it describes qualitatively the decrease in bottom drag with increasing forcing expected on a movable bed (Ardhuin et Al., 2003). The Jonswap's model overestimates wave dissipation over relic ripples and does not describe the sharp increase of bottom roughness where active generation of ripples is expected. The model BT4 doesn't take into account

the tidal currents that should play an important role in the degradation and formation of ripples and also the presence of current should also influence the wave boundary layer. But the available model using currents, like the Grant & Madsen one, have been reported by Tolman (1991) to generate opposite effects to those records by measurements. The BT4 model should be extended to the mud and sand mud mixture to fully reproduce the nature of the bottom.

2.5.   Improvements to open boundary condition

The FIELD_AC project has its main focus is on the coastal zone, where waves, currents and related processes are modelled with an increasing resolution towards the coast. However to account for "fluxes" from the sea side and to bring this information close to the shore, offshore boundary conditions are required to nest the local model into a coarser resolution one implemented for a larger domain (basin).

This boundary condition information will be derived from existing MCS providers (the MyOcean project, recently funded within FP7 GMES is an illustrative case) and from operational centres and project partners. All study sites have access to, or receive, sea boundary data from operational centres.

NOCL Contribution

Various approaches to the specification of open boundary fluxes are used in the FIELD_AC project:

   (i) use of MyOcean data: this can provide the following regional model data.

System	Horizontal coverage and resolution	Vertical levels	Time frequency	Update and time coverage	Parameters
North West Shelf	48N-62N, 12W-13E (following shelf break), 12 km	17 z-levels all variables. 3 level (surface, middle, bottom) physical variables.	Daily mean 17 level, Hourly 3 level.	Daily (target 9:00 UTC), analysis and 5 day forecast	Temperature, salinity, currents, sea level, chlorophyll a, phytoplankton biomass, primary productivity, nitrate, phosphate, dissolved oxygen, optical attenuation
FOAM Global and Regional	Global tiled various (below), North Atlantic (6S-75N) 1/12 deg, Mediterranean 1/12 deg.	43 z-levels (interpolated) except Med, 40 levels.	Daily mean	Daily (target 15:00 UTC), analysis and five day forecast	Temperature, salinity, currents, sea level, sea ice thickness, concentration and velocities

The satellite blended data products are useful for model validation but not suitable for model open boundary forcing due to too coarse spatial resolution. Information on the MyOcean physical model hindcast and forecast can be found at:

- http://catalogue.myocean.eu.org/static/resources/myocean/pum/MYO-NWS-PUM-004-003-v1.1.pdf and http://catalogue.myocean.eu.org/static/resources/myocean/pum/MYO-NWS-PUM-004-001-v2.1.pdf for the NW European shelf and at:
- http://catalogue.myocean.eu.org/static/resources/myocean/pum/MYO2-MED-PUM-006-004-v2.2-1.pdf and http://catalogue.myocean.eu.org/static/resources/myocean/pum/MYO2-MED-PUM-006-001-v2.1-1.pdf for the Mediterranean.

The North West Shelf NEMO model can provide boundary conditions for the Irish Sea/Liverpool Bay model and the German Bight model. The FOAM Mediterranean 1/12 deg model is available for

the Northern Adriatic and Catalan Coast areas. There are monthly mean hindcast products for temperature, salinity, sea surface height and horizontal velocity (meridional and zonal component) from January 1960 – December 2004, with daily mean forecast products from March 2011 to the present. The main limitation of these model outputs is (a) there are no wave data and (b) the daily mean time interval is too coarse.

(ii) use of nested models: most partners are running nested model grids. This is usually necessary when running structured grid models, especially for waves, as no wave boundary model data are available through MyOcean. A nested finite difference model can still be faster than unstructured grid models, and give results of comparable quality to a state of the art finite volume model, and is far easier to pick up and try, both because of its simplicity, and because of the broad base of the user community that has been established.

(iii) use of unstructured grids: the combination of a continuous increase in the power of available computing facilities, together with an interest in modelling sea areas close to complex coastal boundaries means that the flexibility provided by unstructured mesh modelling is proving to have many advantages. FVCOM has been implemented for the Irish Sea, with SWAVE for waves being tested. MIKE 3 grids have been developed for all 4 field cases by DHI. A new unstructured-grid version of MIKE 21 for waves has been tested (DHI Water - Environment - Health).

(iv) the need for regional wave modelling, as an operational product, has been identified leading to initiation of the EU MyWave project, complementing the MyOcean project.
For the pre-operational modelling suite run at NOCL, POLCOMS presently receives boundary data from the UK Met Office FOAM global ocean model. FOAM provides boundary conditions for the AMM model, which in turn forces the open boundary of the Irish Sea domain. Unlike the other data sets, the FOAM data is only for the particular boundary points required. The files come from a model with 34 s-levels (so we get the 32 interior levels); we currently run the AMM model with 42 levels in the COBS operational system, so the FOAM data must be vertically interpolated first. We currently receive daily files which include six days' worth of forecast data. These are not official Met Office products but are supplied to NOCL on a "best endeavour" basis. Thus these are an improvement over the standard MyOcean products.

The FOAM model will be discontinued at the end of December 2012, and we plan to replace the boundary forcing with a new product derived from MyOcean, FOAM-AMM7. The Forecasting

Ocean Assimilation Model 7km Atlantic Margin model (FOAM AMM7) is a coupled hydrodynamic-ecosystem model, nested in a series of one-way nests to the Met Office global ocean model. The hydrodynamics are supplied by the Nucleus for European Modelling of the Ocean (NEMO) with an Optimal Interpolation (OI) data assimilation scheme for sea surface temperature. This is coupled to the European Regional Seas Ecosystem Model (ERSEM), developed at Plymouth Marine Laboratory (PML). The current products available from the MyOcean data portal are too low resolution in both time and space for model downscaling, but work in ongoing to access the full output of the NEMO model.

UPC Contribution:

In our applications in the Catalan Coast, we have used the MyOcean products for the oceanographic boundary conditions and atmospheric forcing. In essence, the products used correspond to the Mediterranean Forecasting System running at INGV. This uses an OGCM (Ocean General Circulation Model) off-line coupled with a wave model and the OCEANVAR data assimilation scheme. It is running every day providing 10 days of forecast and once a week (on Tuesday) 15 days of analysis for the 3D physical ocean. The grid resolution is 1/16 x 1/16 degree and 72 unevenly spaced vertical levels. The variables used in our case correspond to Salinity, Temperature, Sea Surface height, Zonal Velocity and Meridional Velocity. The interpolation to our domain is done using objective analysis for the "father-masked" areas and conservation flow correction at the boundaries. Alternatively, some tests are being carried out with winds from another data source (e.g. MeteoCat, BSC, measured data, etc.). After a comparison with measured data for the Catalan coast we suggest an increase of temporal resolution of Myocean products, in particular the sea surface height, which are associated with pressure gradient, jointly with the local wind, which has an important influence in the shelf dynamics in the Catalan area.

3. Impacts of improved boundary conditions at study sites

3.1.   Introduction

In this section, a choice from the field cases to demonstrate the impact of the different boundary fluxes is shown. As an illustration, for the Catalan coast site the combination of local topography with torrential rain fall can produce considerable local run-off on a very short time interval which might have a large impact on short term local coastal water quality. However, the local rainfall and river run-off are not the only fresh water sources for the Wadden Sea case where the discharge from subterranean estuaries can become significant (distributed run-off). The coupling between modelling and observations will advance the robust specification of these unknown fluxes. For all different study sites, the local partners (HZG, ISMAR-CNR, NOCL, DHI, BSC, SHOM and UPC) have added the last results.

3.2.   Catalan coast

The aim of this section is to show the impact of the introduction of land boundary fluxes on the hydrodynamics of coastal waters. For this purpose the relative importance of different freshwater discharges of the plume and the role of land boundary fluxes in determining the structure of the plume have been studied.

A 3D hydrodynamical model has been set up to incorporate the continental and urban run-off into the Catalan Coastal waters. The model domain includes a small part of the Catalan Coast where the combination of local land topography with torrential rainfall caused considerable local runoff on a short period of time with a large impact on the receiving coastal waters. The Regional Ocean Modeling System (ROMS) simulations were used to examine the dispersal to a freshwater delivery from two relevant events; a low river discharge typical of mean conditions during April 11th 2011 and a high discharge representative of the storm event during March 17th 2011.

Initial conditions for the ocean model fields of currents, depth-averaged currents, water level, salinity, and temperature as well as lateral boundary conditions for currents, salinity, and temperature are obtained from MyOcean products (*http://www.myocean.eu/*). Nested increasing-resolution domains were used in order to introduce these initial and boundary conditions with enough resolution to reproduce the coastal features. The rainfall forecast that is used as input to both the river and urban runoff models to calculate the land boundary fluxes is provided by the Barcelona Super Computing Centre (BSC). It is generated by the WRF-ARW meteorological model

and provides information on the accumulated rainfall per hour in each grid cell of the domain (European, 1km of resolution). Forcing winds have been generated by the meteorological model model; WRF-ARW and provide information of the wind velocity per hour in each grid cell of the domain. The run-off data file that has been used as input file for the coastal model is provided by the conceptual river and urban runoff models that have been calibrated as part of the FIELD_AC project (Keupers et al. 2011). The urban runoff model provides hourly flow time series (m^3/s) for the four combined sewer overflows (CSOs) that are situated in the Coastal model (netcdf format). The river runoff model provides hourly flow time series (m^3/s) for both the Besòs and the Llobregat River.

Impact to freshwater into the coastal waters

An example of the surface salinity differences between results from a simulation without land boundary forcing (March 17th Figure 16, left panel) and a simulation including land boundary forcing (March 17th Figure 16, right panel) is shown in Figure 16. The surface salinity displays big differences mainly close to the two rivers mouth. The impact to include the land boundary fluxes into the coastal water is evidenced in Figure 16.
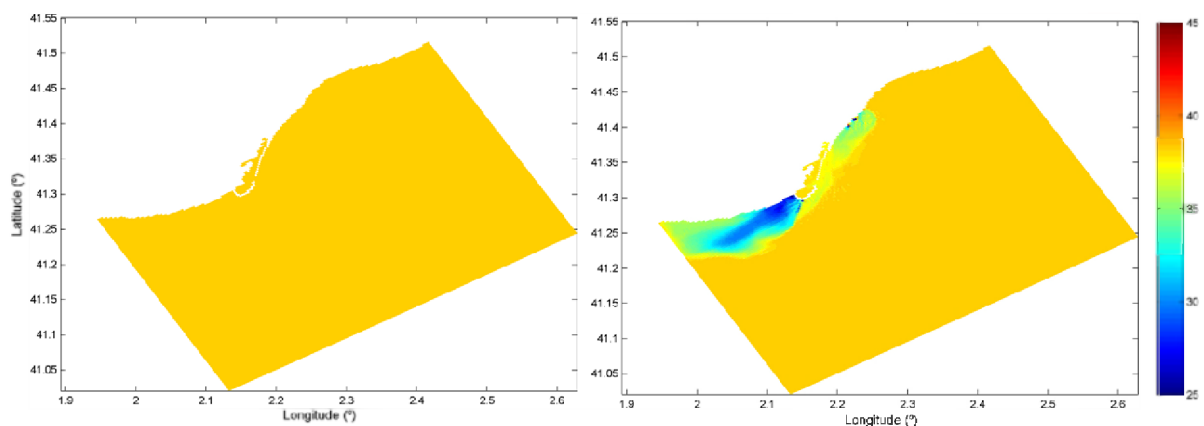
Figure 16. Modelled surface salinity during March 17th without land boundary forcing (left panel) and simulation including boundary forcing (right panel)

Impact to CSO's into the coastal waters

Similarly, Figure 17 shows the salinity fields for a simulation including only rivers as a land boundary forcing (March 17th Figure 17, left panel) and a simulation including rivers and CSOs as land boundary forcing (March 17th Figure 17, right panel). During the flood event (March 17th) the plume spreads offshore in the direction of river water outflow and turned downstream close to the coast.
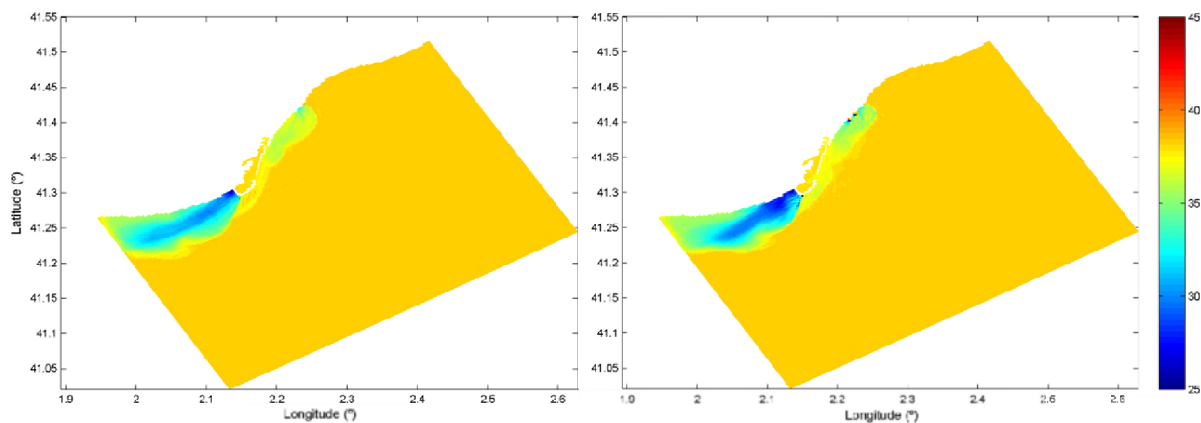
Figure 17. Modelled surface salinity during March 17th including river as a land boundary forcing (left panel) and including river + CSO's as land boundary forcing (right panel).

The impact to include only river or river+CSO's as a land boundary forcing is shown in Figure 18. Figure 18 shows surface salinity differences between results from a simulation including only river outflow as a land forcing (Figure 17, left panel), and the result including river and urban runoff (Figure 17, right panel). This difference suggests that including the urban outflow can play an important role in the spreading and shape of the river plume.
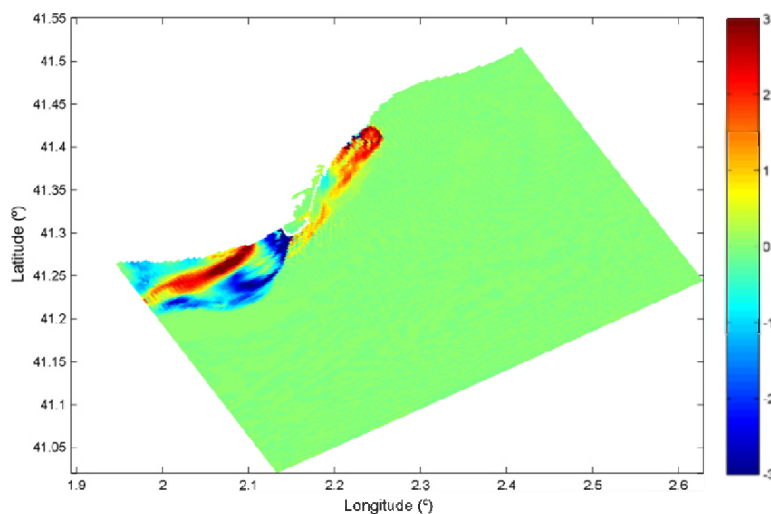
Figure 18. Salinity differences (psu) between the result including the river outflow and the result including river and urban runoff as a land forcing.

Impact to different freshwater flows into the coastal waters

Modelled surface salinity during the two sampling periods (March 17th and April 10th 2011) is presented in Figure 19. The surface salinity exhibits larger spatial variability in March 17th (post-rain conditions, Figure 19, left panel) than in April 11th ('normal' conditions, Figure 19, right panel). In more normal discharge conditions, low salinity water is concentrated around the rivers

mouths. However when a large amount of river water flows into the sea during a flood event, the plume spread offshore in the direction of river water outflow and then turns downstream to remain close to the coast. '
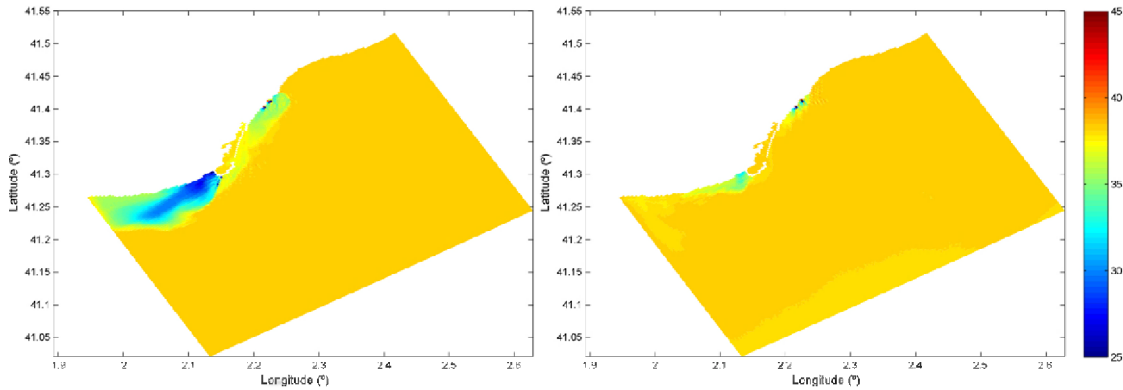
Figure 19. Modelled surface salinity during March 17th (left panel) and April 10th 2011 (right panel)

Impact to different vertical profiles into the coastal waters

Regarding to the three-dimensional structure of the discharge (vertical and horizontal distribution see Figure 20), the model response to different discharge profiles (constant profile, logarithmic profile) has been studied. The model response to different ways of introducing the horizontal discharge needs to be study in more detail. For now, if the river had one cell of the discharge into the grid, all flow was put in this cell but if the river had more than one discharge cell, the flow was distributed as a percentage in each one of cells (Figure 20).
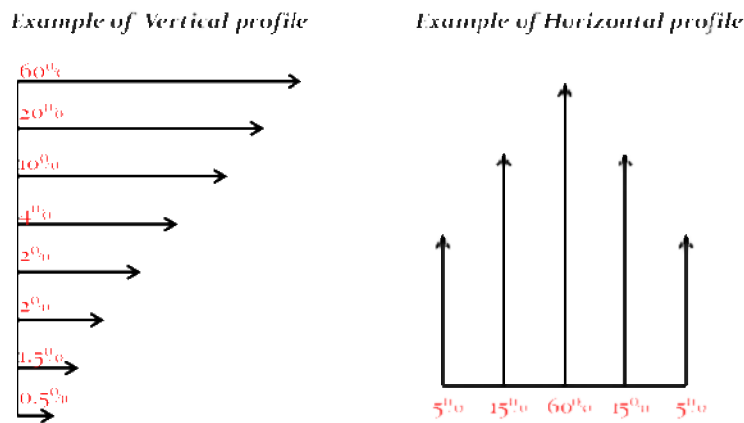
Figure 20. Example of the distributed flow as a percentage in a vertical and horizontal profile that was used to introduce the river discharge.

In Figure 21, the latitudinal profiles around to Llobregat river mouth (Figure 21, left panel) and around to Besos river mouth (Figure 21, right panel) are shown. In both cases, the river outflow plume is clearly visible near to the first layers.
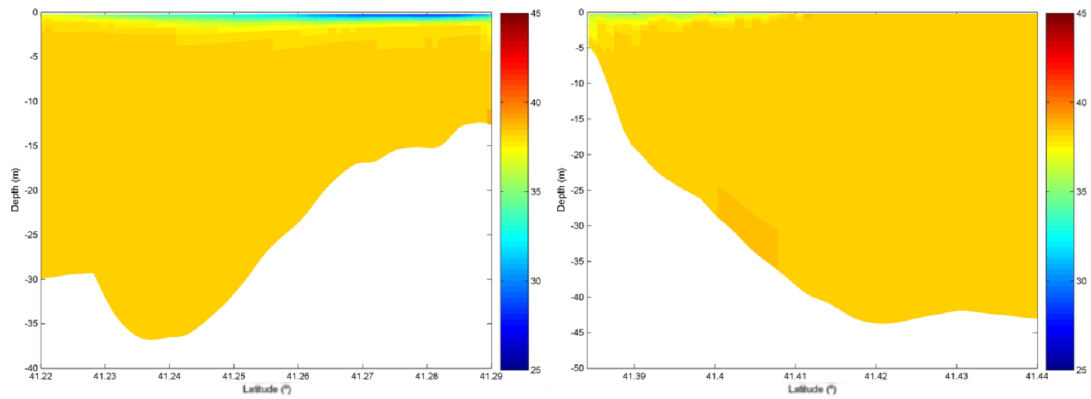
Figure 21. Latitudinal profiles of salinity around the Llobregat River mouth (left panel) and around the Besos River mouth (right panel).

BSC contribution

Impact of high spatial resolution

Three different nested domains have been defined, the inner one at very high spatial resolution: 1) Mediterranean Sea domain (9*9 km), 2) Balearic Sea domain (3*3 km), and 3) Catalan domain (1*1 km) (Figure 22). The impact of the horizontal resolution is addressed comparing the model results on the three domains, focusing on the Catalan Coastal area.

Increasing grid spacing helps to increase the sensitivity of the results. The results show how an increase of the accuracy is obtained from 9*9 km simulations to 3*3 km and 1*1 km simulations (Figure 22). But there are not much differences between 3*3 km and 1*1 km. The increse of resolution improves the realism of the results but not necessarily significantly improve the accuracy of the simulation. In coastal areas spatial resolution is a key point. The dramatic change in bottom roughness when moving from land to sea needs to be sharply represented in models.
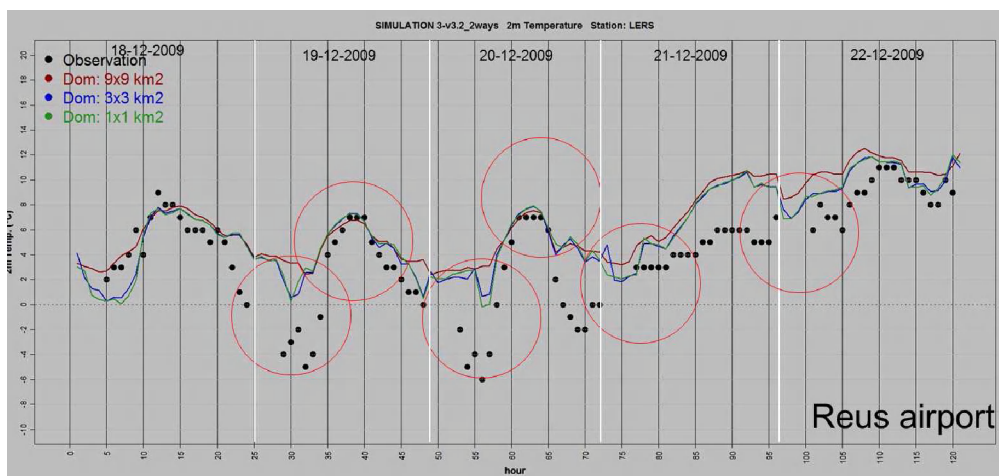
Figure 22. Surface temperature (2m) comparing three spatial resolutions.

Impact to assimilation of Sea Surface Temperature (SST) at high spatial resolution

Impact to assimilation SST from MyOcean compared to SST analysis from NCEP global forecasting system has been analysed. Results didn't bring significant differences between both configurations. It is thought that the selected period was dominated by synoptic situations.

Impact to different physical parameterizations

Related to WRF physics options, two currently used and recommended parameterizations have been compared (YSU and MYJ). No significant differences were obtained related to temperature, wind direction and wind speed. On the other hand, an overestimation of the dew point temperature is observed over coastal and sea areas of the MYJ parameterization that reveals an overestimation of moisture over sea (Figure 23). That's because MYJ is a local closure PBL scheme. Local closure schemes are reported to produce insufficient mixing in the convective boundary layer. Weaker vertical mixing would transfer less surface water vapor to higher layers. This is consistent with previous studies showing that the output of the MYJ scheme was too moist near the surface.
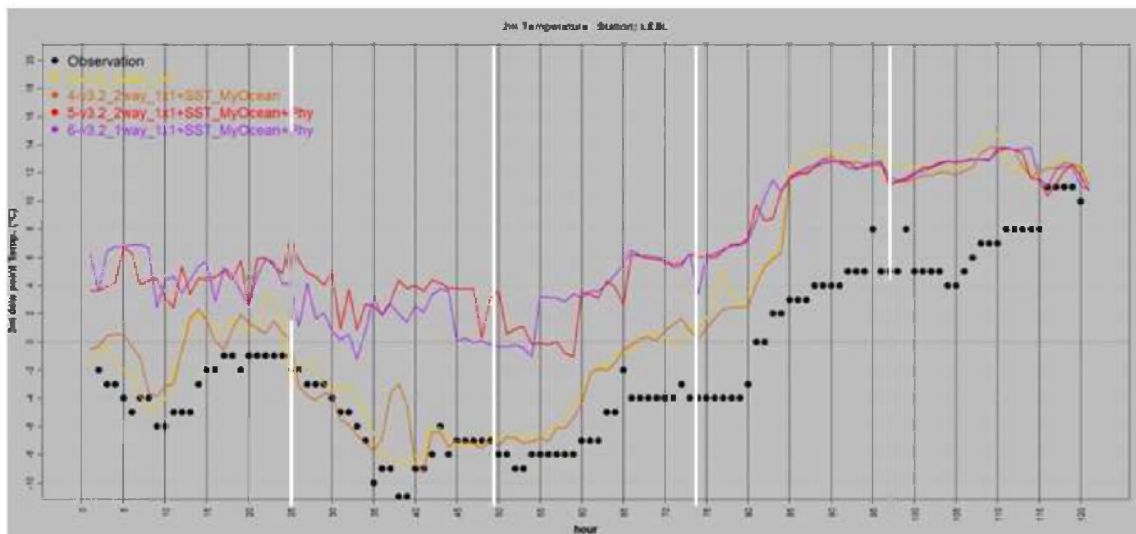
Figure 23. Dew point temperature at Barcelona comparing YSU and MYJ parameterizaitons. MYJ configuration overestimate moisture over sea.

The simulation based on YSU parameterization was compared agaisnt meteorological stations and radar images. Results show that precipitation was very well captured over the entire Catalan domain, especially from the point of view of spatial distribution (Figure 24). The model well reproduced the rainfall depth over the Pyrenees where the annual average precipitation is more

important. Also another important area is the Catalan coast from Barcelona to the Pyrenees where the montain system along the coast leads to significant puntual discharges in summer.

Related to the temporal distribution, the model not only well reproduce the 24h accumulated precipitation but also the hourly distribution. On the other hand, the model slightly underestimates extreme values of precipitation.
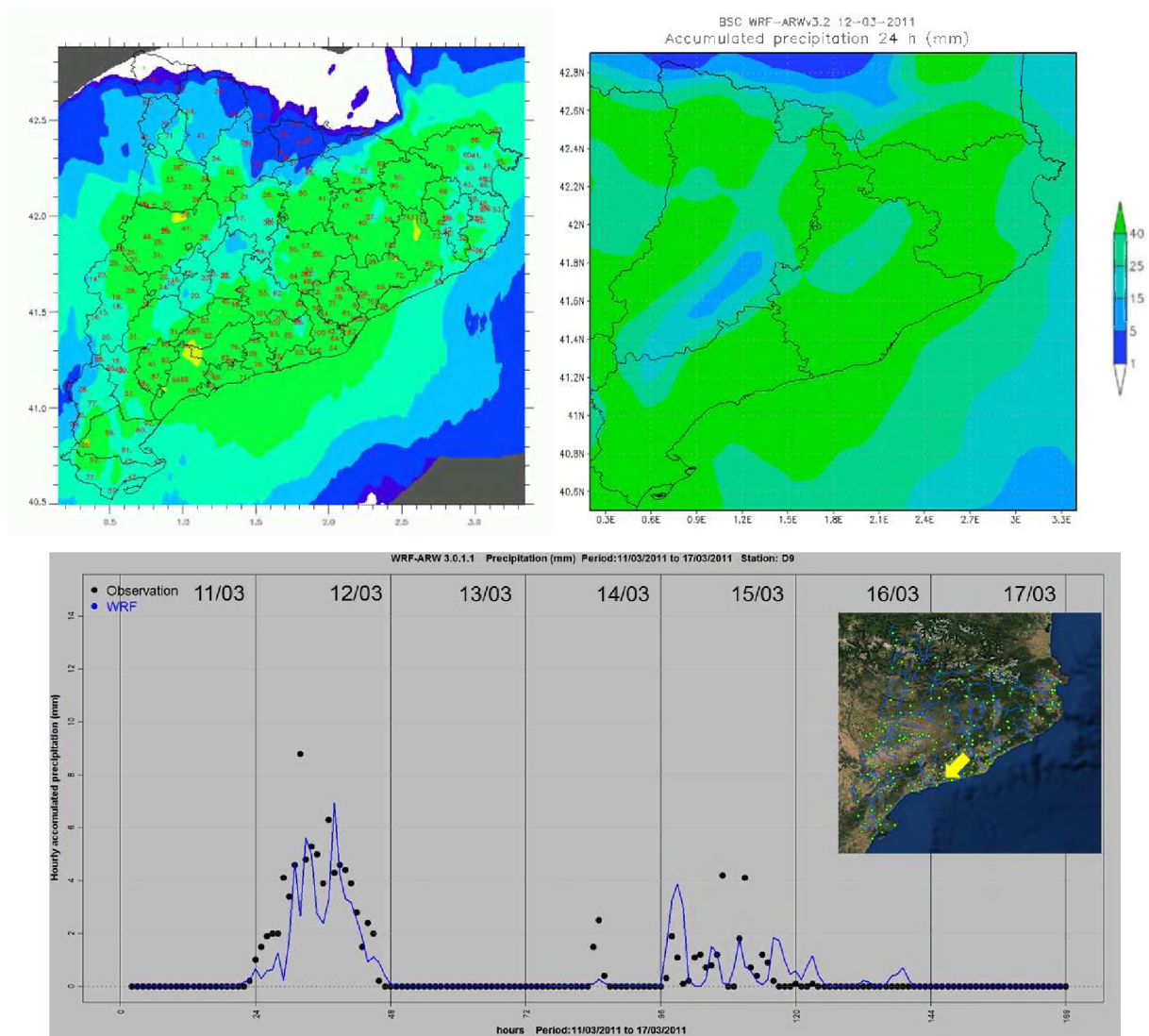
Figure 24. Upper panel: Comparison of 24 h accumulated precipitation over northeast Iberian Peninsula for the 12th March: radar imagery (left) and model estimation (right). Lower panel: hourly precipitation of a station in the Catalan coast (black dots) and model results (blue line).

__Impact to nesting options__

Focussing over nesting techniques, two-way nesting reveals to be a feasible technique for nesting domains. The results don't show significant differences comparing one and two-way nesting. Therefore, from the point of view of the computer resources, specially thinking in a daily forecast system, the 1-way simulations is recommended.

3.2.1. Discussion, limitations and uncertainties

The last examples provide a general interpretation of the impact to include land boundary fluxes into the coastal waters. In the two field surveys carried out at the Catalan coast during the spring of 2011 (during a flood event and during a normal discharge), the impact of a plume to an abrupt change in river discharge was observed. The distribution of low salinity water was different between both discharges. In the normal discharge (April 11th), low salinity water is concentrated around of the rivers mouths. When a large amount of river water flows into the sea during a flood event, the plume spreads offshore in the direction of river water outflow and turns downstream to stay close to the coast. Analysis of the results shows a downward transport of freshwater through vertical mixing was. This was evident during the observation period. The difference between the simulation including the river outflow as a land forcing and the simulation including river and urban runoff as a land forcing suggests that urban runoff plays an important role in the spreading and shape of the river plume.

One of the aspects of river outflow was paid particular attention to when incorporating the 3D structure of the discharge. The model response to different discharge profiles (constant profile and logarithmic profile) has been tested. All results showed a plume that remained in the top layers. It remains to be examined whether an increase the model grid resolution will show significant changes in response to different discharge profiles.

3.3.   Liverpool Bay

__Atmospheric Boundary__

We have begun testing the outputs of the VHM model (provided by KU Leuven). The model has been run for a validation period (January 2004 – December 2010 inclusive). The conceptual hydrological model has been implemented for 12 rivers around Liverpool Bay: Alyn, Elwy, Lune, Clwyd, Irwell, Mersey, Dane, Kent, Ribble, Dee, Leven, and Weaver. The next step is to include the modeled run-off into our hydrodynamic model, and assess the impact of using these data, compared with climatology. Preliminary work on this topic by Jeff Polton (unpublished) suggests

that while the hydrodynamics are sensitive to river input at the coast, the vertical mixing scheme and advection scheme may have more impact on the position of the freshwater front.

Though the horizontal density gradient is salinity controlled, river input temperature has been shown to significantly modulate the plume buoyancy with a seasonal cycle (Polton et al., 2011). Since the open sea has greater thermal inertia than the atmosphere, the sea temperatures lag the freshwater temperature. Thus in winter the sea is generally warmer than the estuaries, whereas in summer the estuaries are generally warmer than the sea. The freshwater always makes the estuaries plumes positively buoyant, but the 4°C temperature variation means that in the summer the density stratification is enhanced. There is a tendency in POLCOMS for a too strong horizontal density gradient as well as a pronounced vertical stratification. Salinity and temperature are directly measured by an instrumented ferry as it leaves the Mersey for Ireland. Setting the freshwater to have a temperature seasonal cycle that matches the Mersey Narrows annual cycle, as measured by the ferry, produces qualitatively improved plumes compared with setting the estuarine water to simply match the ambient sea water temperature.

Bottom friction

Wave–current bottom friction is calculated in WAM using Madsen's (1994) method by default, the bottom roughness is then imposed within POLCOMS, allowing a 2-way interaction in the bottom stress to be calculated (Osuna and Wolf, 2005). Waves enhance the bottom roughness increasing the frictional influence on the current field. Without wave influence a constant bottom roughness length, with a default value of 0.003 m in Liverpool Bay, is used. However in recent work by Brown (2010) it was found necessary to reduce the bottom friction experienced by waves in very shallow water, comparing the model output from SWAN and WAM to the Triaxys buoy near Hilbre Island in the Dee Estuary. In the SWAN wave model, the bottom friction is implemented as a choice of wave-alone formulations, even when currents are included, since results found by Tolman (1992) suggested that currents have no effect on wave-induced bottom friction. The default JONSWAP model (Hasselmann et al., 1973) was found to give good results in very shallow water (Booij et al., 1999) and is also available in WAM. The constant bottom friction coefficient applied takes a default wind sea value (0.067 m^2s^{-3}) in SWAN, but a lower (swell wave) value (0.038 m^2s^{-3}) in WAM. The swell wave setting was found to give more accurate wave heights in the Dee Estuary under storm conditions and was therefore imposed in both models. The over predictions in the offshore significant wave height for uncoupled and coupled models (Figure 25 a) may be accounted for by the overestimation in the wind speed, however in the nearshore the significant wave height is

under-predicted. This implies that the balance between energy input and loss in the activated model source terms becomes less accurate in shallow water. The need to reduce the energy loss may explain the need for a reduced bottom friction coefficient in shallow water.
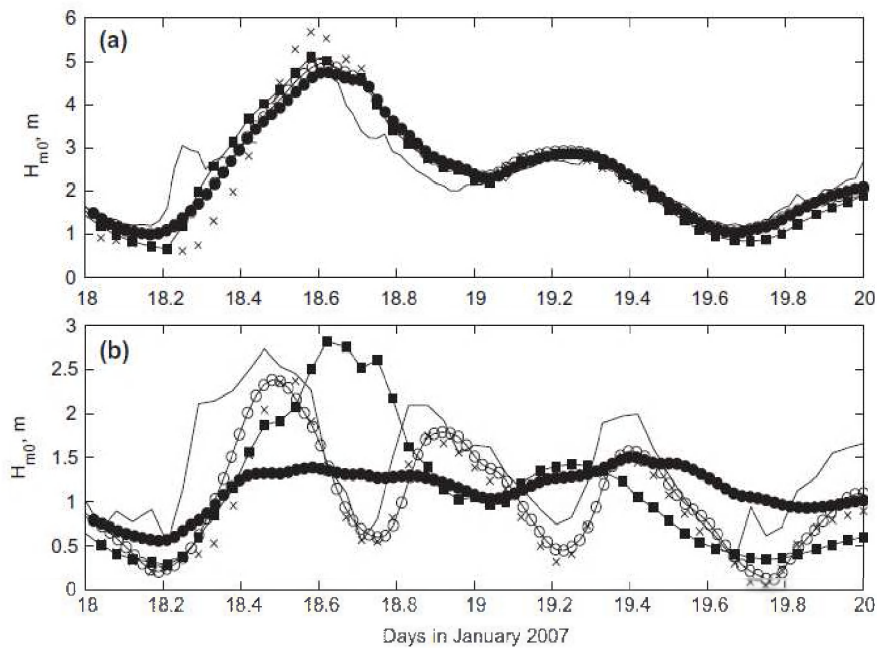
Figure 25. The offshore (a) and nearshore (b) significant wave height, Hm0, observations (solid line) compared with the 1-way coupled POLCOMS–ProWAM with relaxed limiter hindcast and reduced JONSWAP bottom friction (crosses), the 1-way coupled POLCOMS–SWAN hindcast with reduced JONSWAP bottom friction (line with unfilled circle symbols), the uncoupled ProWAM hindcast with Madsen wave-alone bottom friction (line with filled square symbols) and the uncoupled SWAN hindcast with reduced JONSWAP bottom friction (line with filled circle symbols) (from Brown, 2010)

3.3.1. Discussion, limitations and uncertainties

Experience in modeling Liverpool Bay has identified the important influence of the freshwater input from the rivers in the area in controlling the ROFI dynamics. The move from climatological river input t(with little seasonality) to the inclusion of the larger pulses of freshwater due to periodic heavy rainfall (not necessarily in winter/spring) brings more realistic results. However the details of the freshwater plume are difficult to model, partly due to model numerics, in correctly modeling advection and mixing of the fresh water, and partly due to lack of detailed knowledge of the temperature of the river water, and the estuarine processes.

The offshore boundary forcing has much improved by having available higher frequency forcing from the UK Met Office, rather than the standard MyOcean products.

The atmospheric input has been improved by running the WRF model at higher spatial resolution than available from the standard Met Office forcing.

Wave-current coupled bottom friction has been used typically in the POLCOMS-WAM model but recent results from Brown (2010) have suggested that this over-estimates the bed stress and so under-predicts the wave height. Better results may be obtained with the JONSWAP friction with the lower, swell wave, friction coefficient.

3.4.   German Bight

The assessment of the impact of improved boundary conditions in the German Bight was studied mainly using the three dimensional primitive equation model GETM. A detailed description of the model was given in deliverable 2.3 (Bricheno and Wolf, 2012).

The nested-grid model consists of three model configurations: A coarse-resolution North Sea-Baltic Sea (~ 3 nm) outer model, a fine-resolution (~ 1 km) inner model covering the German Bight and two finer resolution (~ 200 m) models for Elbe rive region and (~ 50 m) for the East Frisian the Wadden Sea region – and for the Sylt-Römö Bight, resolving the barrier islands and the tidal flats as well.

The model system is forced by: 1) the atmospheric fluxes estimated by the bulk formulation using 1-hourly forecast German Weather Service (DWD), 2) hourly river run-off data provided by the BSH operational model, and climatological data for the 30 most important rivers within the North Sea- Baltic Sea model area provided by the Swedish Meteorological and Hydrographical Institute (SMHI), 3) time-varying lateral boundary conditions of sea surface elevations temperature and salinity. The sea surface elevations of the open boundary of the North Sea-Baltic Sea model are generated using tidal constituents obtained from the TOPEX/Poseidon data via the OSU Tidal Inversion Software. Temperature and salinity at the open boundary of the outer model are interpolated at each time step using the monthly mean climatological data. Alternatively, lateral boundary conditions from the operational forecast model of the German Federal Maritime and Hydrographic Agency (BSH) are used.

Only for the impact study on high resolution wind fields the wave model WAM was used, since wave modelling results are heavily dependent on the forcing wind fields. The test case was run on the coarse resolution North Sea – Baltic Sea setup.

The role of the meteorological forcing, extreme events

In this section we aim to study the response of the German Bight thermo- and hydro- dynamics on extreme events. As a test case we choose the extreme storm Britta. The Hurricane "Britta" on 1st November 2006 is assumed as one of the worst for the last 100 years in the lower Saxony German coast (Figure 26).

Figure 26. Hurricane Britta effects.

The analyses of the available meteorological forcing (NCEP, ECMWF, DWD) showed that for the "Britta" storm the temporal and spatial resolution of the NCEP data were not sufficient to match the observed wave or current velocity conditions. Therefore, atmospheric data with a higher temporal and spatial resolution have been taken from the German Weather Service (DWD) for the North Sea and the Wadden Sea.

Figure 27 demonstrated the meteorological conditions during the storm Britta over the North Sea .It is clearly seen that during that event for the southern part of the North Sea the dominating wind is characterized not only by a very strong magnitude but also by a persistent southern direction (towards the East Frisian Wadden coast). Due to the favourable meteorological condition this storm caused strong damages on the East Frisian German coast.
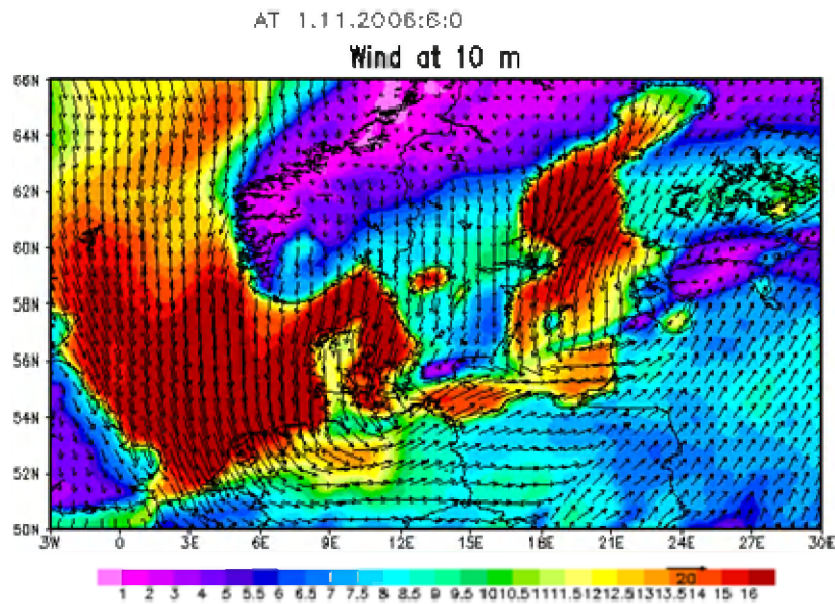
Figure 27. The meteorological conditions during the storm Britta

The storm surge on 1 November 2006 caused a sea level rise that ranges among the three highest sea levels ever recorded along the Lower-Saxionian coastline over the last 100 years (1906, 1962, and 2006). Furthermore, storm Britta caused extremely high waves in the German Bight, as evidenced by structural damage to the FINO1 wind farm research platform (45 km offshore) at heights up to 20 m above the mean sea level (see e.g. Emeis and Türk 2009, and references therein).

For the numerical simulations of storm Britta, the sea level, temperature and salinity boundary data were extracted from an external modelling system for the German Bight. We use the same atmospheric forcing data for both the German Bight and Wadden Sea set-up.

As can be seen from the Figure 28 and Figure 29, the model is capable to simulate both the variability and the magnitude of the sea level in the Wadden Sea and the German Bight The sea level height on 01.11 was about three times larger than the typical one for the Wadden Sea region Even more, during the extreme event period the very shallow coastal areas, which are normally dry during ebb were always covered with water (compare Figure 29 b and Figure 29 d)
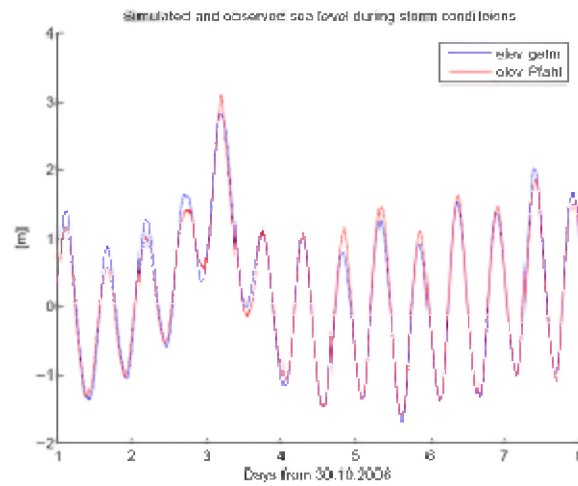
Figure 28. Simulated (blue line) and observed (red line) sea level (m) during Britta storm at time series station "Watt". X-axis corresponds to the time (days from 30.10.2006).
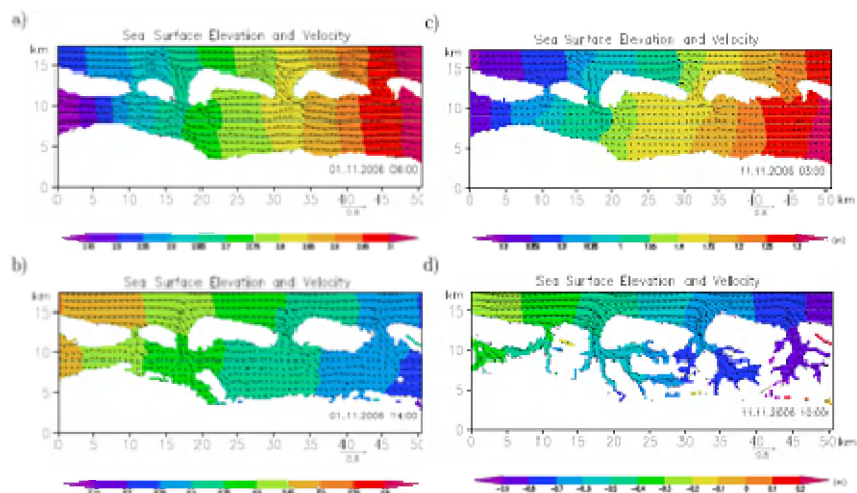
Figure 29. Sea Surface elevation and velocity for the East Frisian Wadden Sea during extreme event Britta by (a) high water on 01.11.2006 (b) low water on 01.11.2006; and in the normal situation 10 days later (c) high water on 11.11.2006 (d) low water on 11.11.2006.

The evolution of the vertical profiles of temperature, salinity and potential density at the time series station "Watt" is shown on Figure 30. One can clearly see the changes of the stratification of the "Britta" event. Before 01.11.2001 the water column was well homogenized. However, after the storm, the column appears to be well stratified. This is better pronounced during the low water. The simulated bottom temperature was much lower than the surface one. Consequently, the potential density at the bottom is much higher than the surface one and therefore the vertical gradients significantly increased making the water column highly stratified.
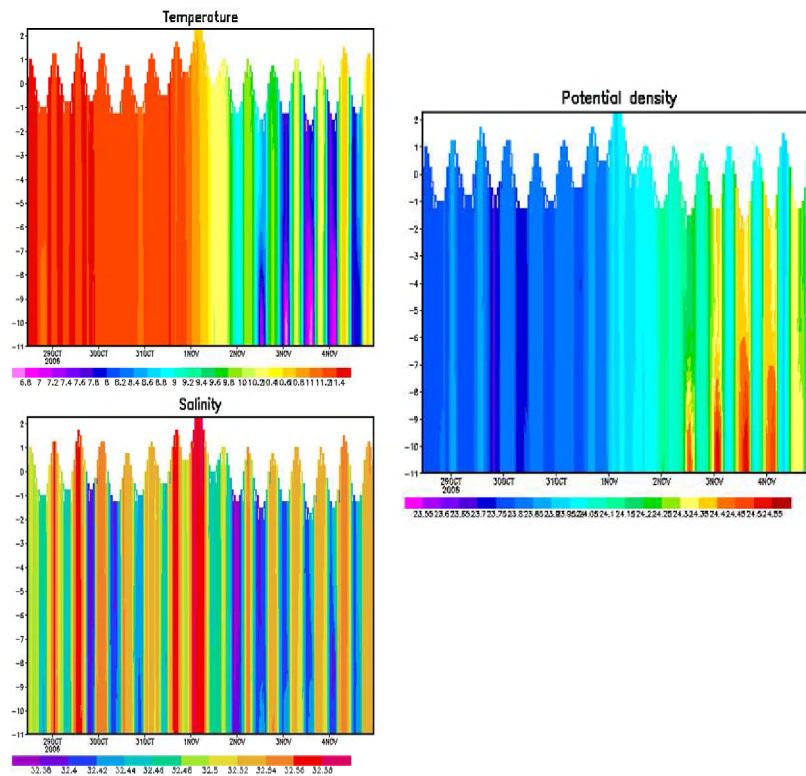
Figure 30. Evolution of the vertical profiles of temperature, salinity and potencial density *at the time series station "Watt". Y- axis corresponds to the depth (m), x-Axis to the time. The variable depth at the sea surface is due to the variability of the sea surface elevation.*

Using the numerical model we aimed to study the reasons for changing of the vertical stratification after the extreme storm. From Figure 31 it is clearly seen that the atmospheric temperature over the Wadden Sea drops of about 6 degree within only several hours on the 01.11. Additionally, the wind magnitude increased significantly and its direction changes to southward during the extreme storm. Were these stratification changes due to changes of atmospheric temperature or due to the wind forcing? To answer this question we performed several sensitivity experiments (see the Table 2) in which we filtered either the atmospheric temperature (Exp. 2), keeping the realistic wind forcing, or filtered the wind, keeping the air temperature realistic (Exp.3), or filtering both the air temperature and the wind (Exp. 4). Then we run the nested. -grid model for the German Bight and East Frisian Wadden sea set-ups for a one month period, starting at 15.10.2006.
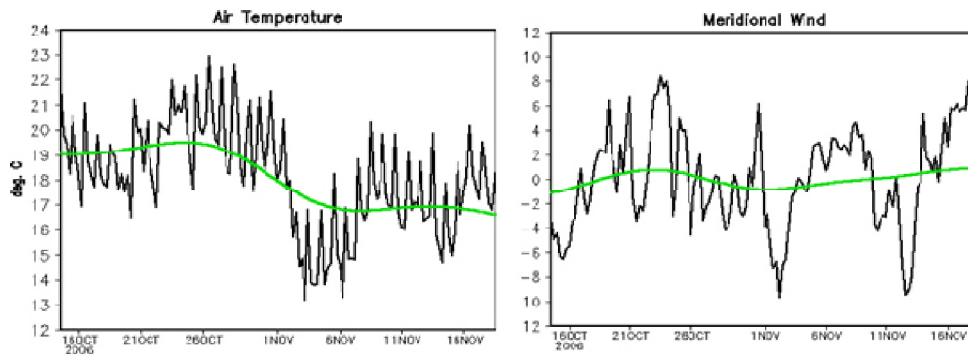
Figure 31. Time series of the meteorological forcing at the station Watt": air temperature (left), wind (right). The Black line corresponds to the real data, the green - to the filtered one.

Experiments	Air Temperature	Wind
Exp. 1	Real	Real
Exp. 2	Filtered	Filtered
Exp.3	Real	Filtered
Exp.4	Filtered	Read

Table 2. Table of the experiments
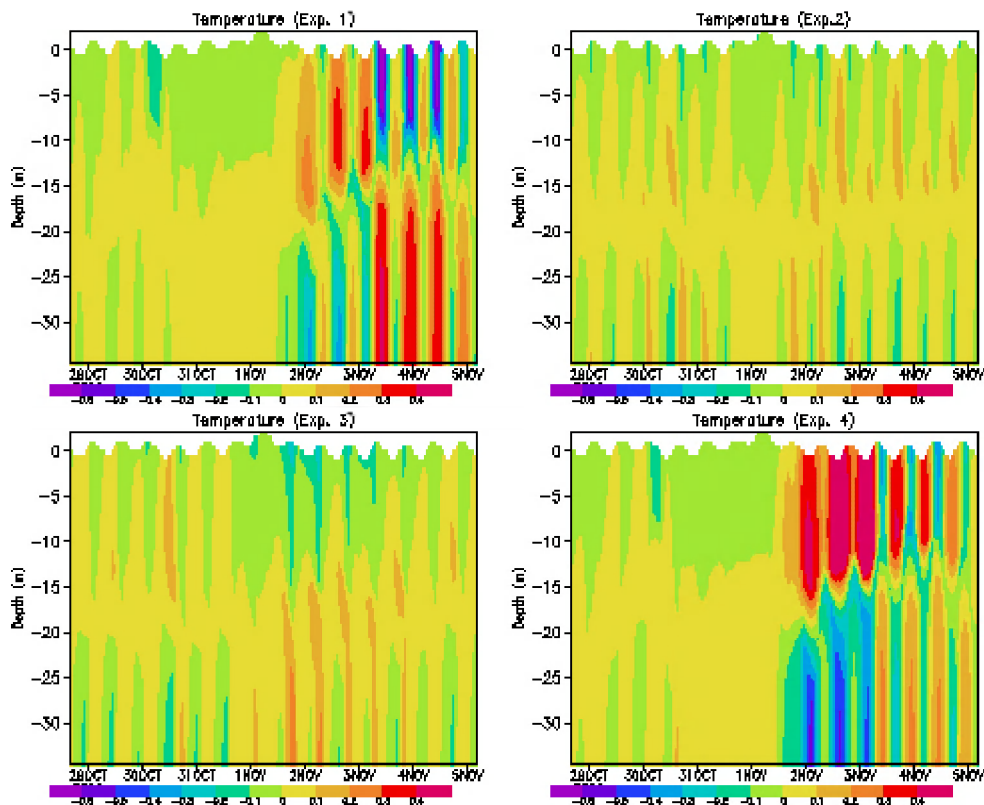
Figure 32. Evolution of the vertical profile of the temperature anomaly at 53.8 deg. N, 7.7 deg E for the four sensitivity experiments.

The role of the atmospheric forcing

Another series of experiment that we performed for the German Bight is to study the sensitivity of the model to the atmospheric forcing. The table bellow (Table 3) described the different experiments performed during the October and November 2011. The initial conditions for all three experiments are the same taken from the main run (Exp. 1), in which we use the DWD (German Weather Service) atmospheric data with 1hr time discretisation. The River runoff forcing for this experiment is taken from the hourly data provided by the BSH (German Hydrographical Service). In the second experiment we substitute the DWD atmospheric forcing with a climatological monthly mean one. The river run-off forcing is the same as in the main experiment. In the third run we keep the atmospheric forcing the same as in the main experiment but switch off the river forcing. Figure 33 shows the Sea Surface Temperature (SST) difference averaged for October and November 2011 between the sensitivity experiments. The role of high frequency atmospheric forcing is clearly seen, especially for the coastal areas of the German Bight. On the other hand, the river run forcing influence is observed not only in the regions near the major German Bight Rivers but also off shore. The change of the baroclinicity due to the river run-off changes the vertical stratification and thus reflects the sea surface temperature as well.

	Atmospheric forcing	River forcing
Experiment 1	Realistic	Realistic
Experiment 2	Climatological	Realistic
Experiment 3	Realistic	Not included

Table 3. Table of the experiments with different atmosphere and river forcing
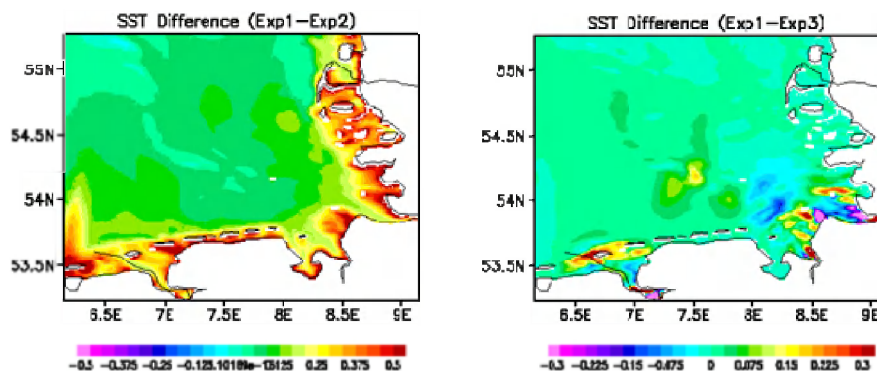
Figure 33. Sea Surface Temperature (SST) difference (deg. C) averaged for October and November 2011 between the sensitivity experiments to the atmospheric and river forcing, as described in the Table 2.

Incorporation of Land Discharge Runoff into Oceanographic Models

The fresh-water fluxes from the three main tributaries in the region are taken from the observations available from the Niedersaechsischer Landesbetrieb fuer Wasserwirtschaft und Kuestenschutz, Aurich, Germany. These measured data are interpolated within GETM at each time step in order to obtain a smooth input. Besides these measured river data, five additional tributaries were specified for the East Frisian Wadden Sea set-up (T1-T5) (Figure 34). The value of fresh water flux imposed

Tributaries	Fresh water flux run-off (m3/s)
T1	36.3
T2	9.13
T3	25.11
T4	25.11
T5	40.0

at these locations is given in Table 4.
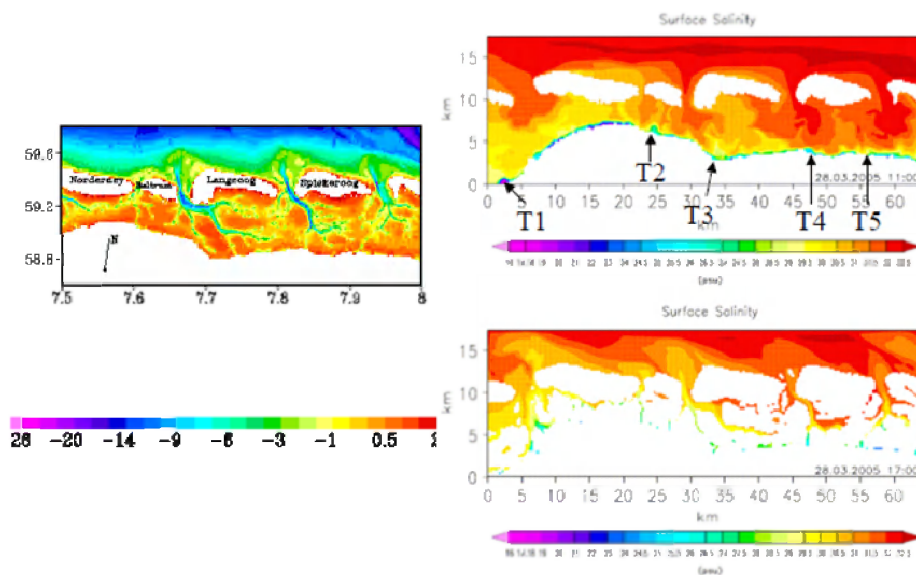
Figure 34. East Frisian Wadden Sea bathymetry (left) and surface salinity during high (28 March 2005 11 UTC) and low water (28 March 2005 17 UTC) (right). The location of the five tributaries (T1-T5) is specified.

Tributaries	Fresh water flux run-off (m3/s)
T1	36.3
T2	9.13
T3	25.11
T4	25.11
T5	40.0

Table 4. Table of the experiments with different fresh water flux.

Additionally along the whole Wadden Sea coast a ground water flux of 0.2 m3/s along the southern coast (324 point) is specified.

Role of the atmospheric forcing and density stratification

Figure 35 shows time-averaged surface current, vertically averaged current and vertically integrated transport (vertically averaged current times local depth) for the German Bight during September 1991. This presentation of circulation is needed in order to illustrate the field, which we further analyse, that is the surface current (Figure 35 a), and to give an idea about consistency between surface and vertical mean current or transport. Obviously the three patterns reveal different characteristics of the circulation. It is noteworthy that the surface current has a pronounced maximum along the southern coast and shows a convergence from west to east.

Absolute maxima are located in the regions of straits connecting intertidal basins with the open ocean. Vertically averaged current (Figure 35 b) is qualitatively similar to the surface current. However, along the western model boundary the meridional component is much stronger. The dominating zonal transport in the surface current in the interior of the model area is substituted by a northward transport in the pattern of vertically averaged current. In both plots the region around the island of Helgoland shows a pronounced regional pattern.

The Eulerian time-mean vertically integrated circulation in most of the German Bight area is cyclonic, which is mainly due to the dominant eastward wind forcing, i.e., a circulation in the direction of propagation of the tidal wave (from west to east along the southern boundary and from south to north along the coasts of Germany and Denmark). A local minimum of the circulation occurs in the coastal East and North Frisian Wadden Sea. The vertically integrated transport displays to a larger extent the characteristics of the German Bight topography, which is dominated by the underwater extension of the Elbe Estuary. The northern bank of this estuary reduces substantially the penetration of open ocean waters into the shallow coastal zone, and consequently the direction of incoming flow turns abruptly to north northwest. The question of the role of density for the circulation in the German Bight has been addressed by Carbajal and Pohlmann (2004); however their work focused primarily on the modification of characteristics of tidal ellipses. We assume that further attention has to be paid to this question, in particular because the region is a typical representative of ROFI. It is still not quite clear what the joint role of wind and density for

the regional circulation is. Therefore, along with our main numerical simulation (for brevity "realistic" run), we also performed a simulation with constant temperature and salinity (for brevity "constant density" run).
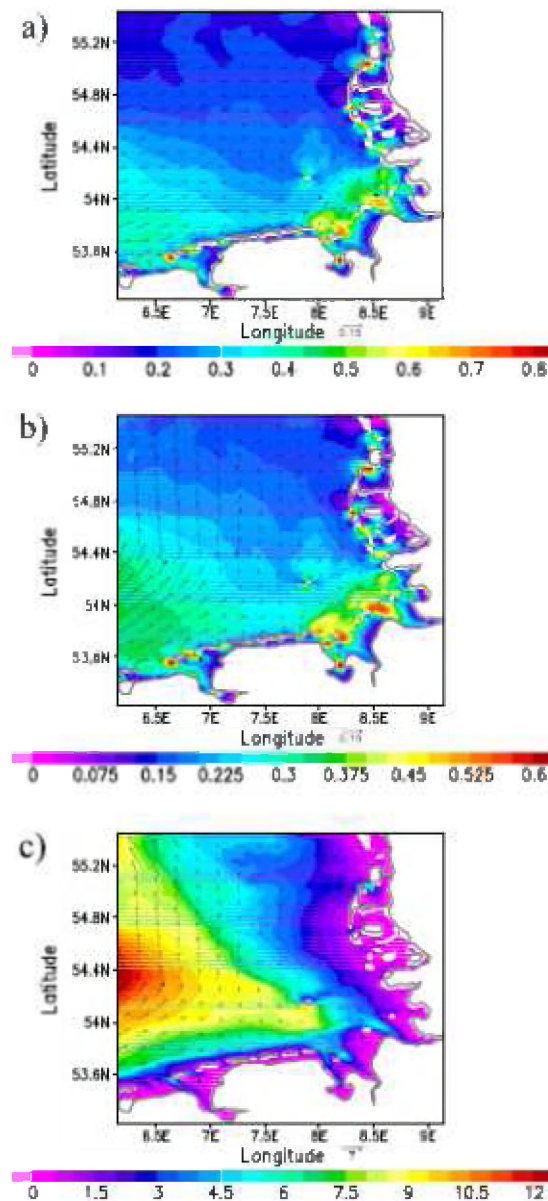
Figure 35. Eulerian time-mean of currents simulated by the German Bight model for September 1991: a) surface currents (m/s), b) vertical mean of currents (m/s) and c) vertically integrated currents (m2/s), colour-coded according to the colour bars. The arrow below each plot corresponds to current or vertically integrated current in m/s or m2/s, correspondingly.

By examining the difference between these two experiments we want to illustrate the motivation for the analyses provided below. We discuss below the correlation between surface current and wind. Two analyses are presented: (1) analysis on the correlation between total current velocity and wind,

and (2) analysis of the correlation between non-tidal residual velocity and wind. It appeared that the large variability due to tidal currents make the correlation too weak. Unlike the theoretical case of Ekman currents, which is applied to an infinitely deep ocean, our model area is a mix of very shallow coastal areas, where the surface current is supposed to follow wind direction and depths bigger than the Ekman depth. The preliminary expectation is that the correlation between wind and surface currents will replicate topography changes, however the effects of density are not trivial and difficult to specify in advance. Analysis of the realistic and constant density runs is presented below first by the complex correlation between the different surface velocities in the two experiments and wind (Figure 36 a). The result is not trivial. It appears that the effect of density results in an increase in the magnitude of complex correlation in an area around the island of Helgoland and extending to the northern model boundary, while changes are minimal in the shallow coastal areas and in the southwest of the domain. As demonstrated by additional analyses of individual velocity components (data not shown) this result is mostly due to meridional velocity. Subtracting the tidal prediction, the non-tidal residual surface currents show a high correlation with wind (Figure 36 b and Figure 36 c). It is noteworthy that low magnitude of complex correlation in front of river mouths in the experiment with constant density has nothing to do with the river runoff. Obviously, these mesoscale features are a result of complex coastal line and bathymetry, which acts almost in the same way in the two experiments. This could be used as a demonstration that even in this very simple case (constant density) impact of wind on the circulation is not trivial.
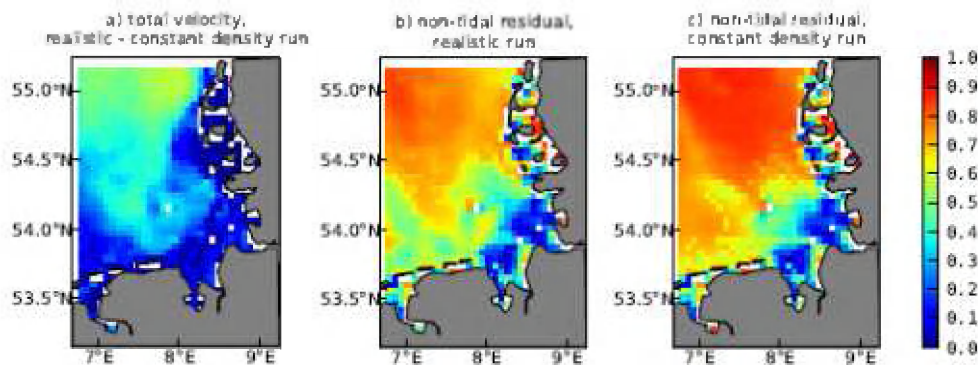
Figure 36. Magnitude of complex correlation of different numerical simulation surface velocities with wind. From left to right, the numerical simulation data is: a) the difference between total surface velocity in the realistic and constant density runs, b) the non-tidal residual surface velocity in the realistic run and c) the non-tidal residual surface velocity in the constant density run.

The role of baroclinicity is well illustrated in the difference between Figure 36 b and c. Overall, in the presence of density stratification the correlation decreases, which is actually more pronounced

in the zonal than in the meridional component (data not shown). The role of density changes when we analyse non-tidal residual currents compared to the case when we include tidal oscillations in the correlation analysis. This is consistent with the approach taken by Kundu (1976), who removed tidal oscillations from his analysis. The general trend for non-tidal residual currents is a decrease of their correlation with wind in the realistic run compared to the constant density run, while the trend derived from the analysis of the total currents is not so simple. This gives an indication that in the presence of tides the instantaneous velocity field could show a rather complicated response to wind forcing. The explanation of the difference between plots from the two experiments in Figure 36 b and c is facilitated, if we analyse the differential Eulerian time-mean velocity (Figure 37). Overall, the increase of mean velocity in the central part of the model area due to density is comparable to the Eulerian time-mean residual velocity (see Figure 35). Furthermore, change in the direction of currents from the realistic experiment to the one with constant density is such that density tends to detect current velocity in the interior of the model area to the right. On the contrary, in the coastal zone an opposite direction is observed. The spatial variability of correlation between surface current and wind is indicative for the work done by wind. From the numerical simulations it is obvious that this measure of mechanical forcing is quite complex. It is highly dependent on density, with corresponding patterns changing dramatically over short distances. Most of these changes occur in the coastal zone covered by HFR observations as demonstrated by Port et al (2011). This gives us the motivation to further investigate the consistency between observations and numerical simulations focusing on regional patterns.
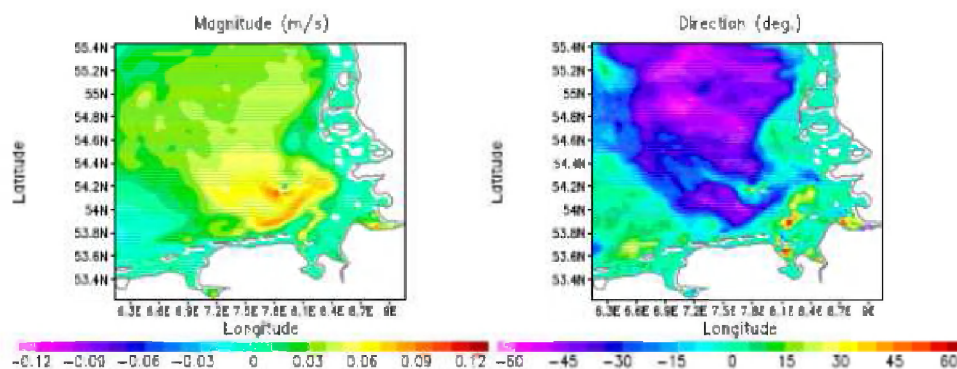
Figure 37. Difference between Eulerian time-mean velocity magnitude and direction in two experiments (realistic run minus constant density run), magnitude in m/s and direction in degrees colour-coded according to the colour bars.

Impact of MyOcean open boundary conditions

The impact of the open boundary forcing was studied using the German Bight setups with 1 km resolution. Boundary values were taken either from data of the German Federal Maritime and Hydrographic Agency (BSH) or from MyOcean products. The MyOcean data are from the North West Shelf marine forecast centre (MFC) and were generated with the FOAM model with 7 km spatial resolution. The MyOcean NWS product for water levels and currents contains 3 vertical levels and has hourly time steps. Both clamped and Flather boundary conditions for the barotropic part were used for the forcing at the open boundaries.
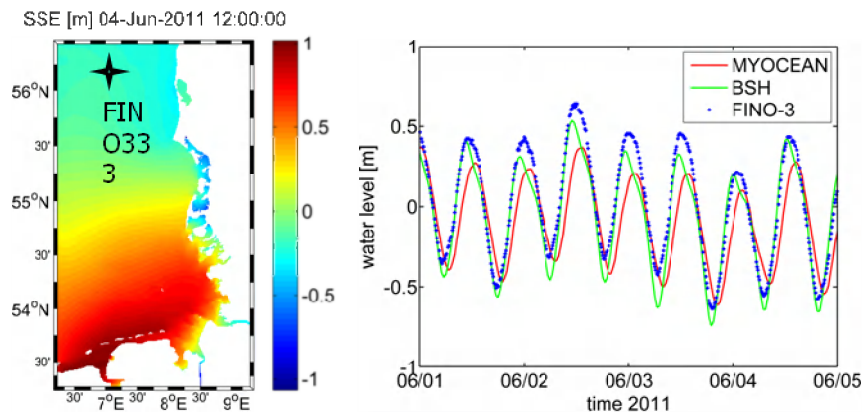
Figure 38. Comparison of modelled (with MyOcean and BSH boundary forcing) and measured water levels at FINO-3 (right). To the left a snapshot of the water levels in the model area is shown, the position of the FINO-3 station is indicated.

A snapshot of the water level for June 4, 2011 12:00 UTC from the run with MyOcean boundary data is shown in Figure 38 (left). Figure 38 (right) shows a comparison of water levels computed with the GETM model using BSH and MyOcean boundary data with pressure sensor measurements taken at the FINO-3 platform (56.195N 7.158E). One can see that the BSH data forcing appears to provide more consistent results for this area as far as the barotropic part is concerned.

Impact of high resolution wind forcing

For a first comparison of wave modelling results on high resolution wind fields the wave model was run in the outer model area using COSMO-DE (spatial resolution 2.8 km (0.025°)) and COSMO-EU winds (spatial resolution of 7km), respectively. The data were provided by the German Weather Service (DWD).
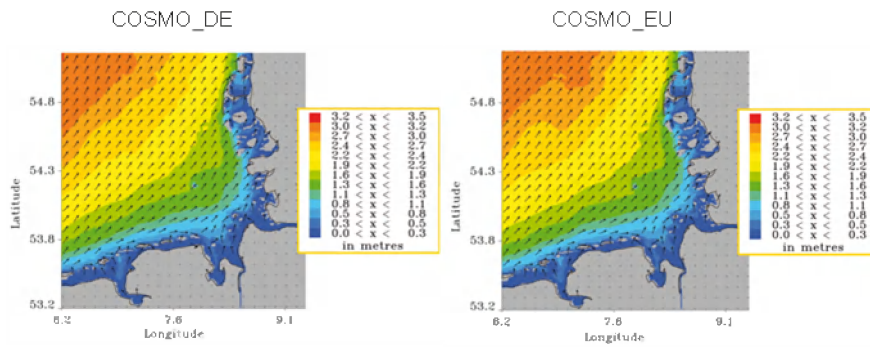
Figure 39. Significant wave height and wave direction in the German Bight model area when forced with COSMO_DE (left) and COSMO_EU (right) winds, respectively.

Figure 39 shows a snapshot of the resultant significant wave heights and directions. In the northern part of the North-Sea little differences in wave height can be observed, whereas wave direction seems to be unaffected throughout the model area. Future studies will clarify whether these findings are representative.

Impact of wave forcing on hydrodynamic modelling results

The German Bight is characterized by wind-waves and strong tidal currents.

As a result, effects such as nonlinear feedback between currents and waves play an important role in this area results, especially in coastal areas like the Wadden Sea and estuaries: wave friction will affect the tidal current profiles in shallow areas and may deepen the surface mixed layer. The transfer of momentum by waves becomes important for the mean water level setup and for alongshore currents (wave breaking) generated by waves in the surf zone.

To include wave effects in GETM the original version was modified to account for the depth dependent radiation stresses and Stokes drift. The gradient of the radiation stresses serve as additional explicit wave forcing terms in the momentum equations for the horizontal velocity components. The Stokes drift was subtracted from the wave force in order to transfer it to the Eulerian framework. In the GOTM turbulence module which is coupled to GETM the dynamic k-epsilon style equation was chosen. As boundary condition for the upper boundary layer injection of turbulent kinetic energy due to breaking waves was implemented.

To assess the impact of wave forcing on hydrodynamic results the GETM German Bight model was run with and without wave forcing for February 2012.
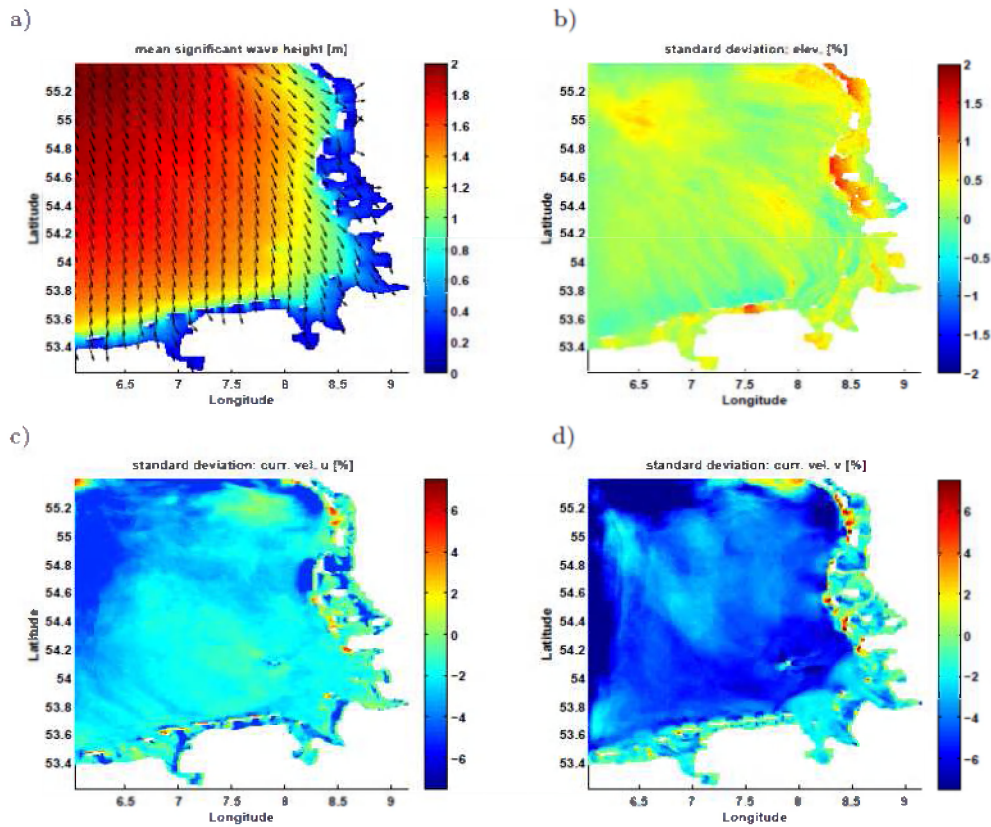
Figure 40. Impact of wave forcing in the German Bight: standard deviation of (b) water level and (c,d) surface currents). Averaged values for one month (February 2012). Additionally, the average wave heights and directions are shown in (a).

Figure 40 shows the averaged standard deviations between the two runs. The average wave height in the period was about 2m in the open North Sea coming from North. Near the coast water levels rise up to two percent, especially in the East. The meridial surface currents are slowed down due to turbulence up to six percent in the North Sea whereas the zonal component is much less affected. Near the coast and in particular between the islands alongshore currents are generated by the wave forcing, increasing the average values up to six percent.

Impact of higher resolution on estuarine modelling

The Elbe river region model was used to study the generation of tidal intrusion fronts along the deepest part of main the channel system. The model predicted a shear front formation during ebb phase and tidal intrusion front during flood phase. The results from the numerical model showed that the strong slope topography was a main factor for the generation of the tidal intrusion front. Different grid model resolutions of 400m and 200m were used. The model results were validated against observations (see Figure 41) of phase and tide amplitude of the major tide constituents M2.
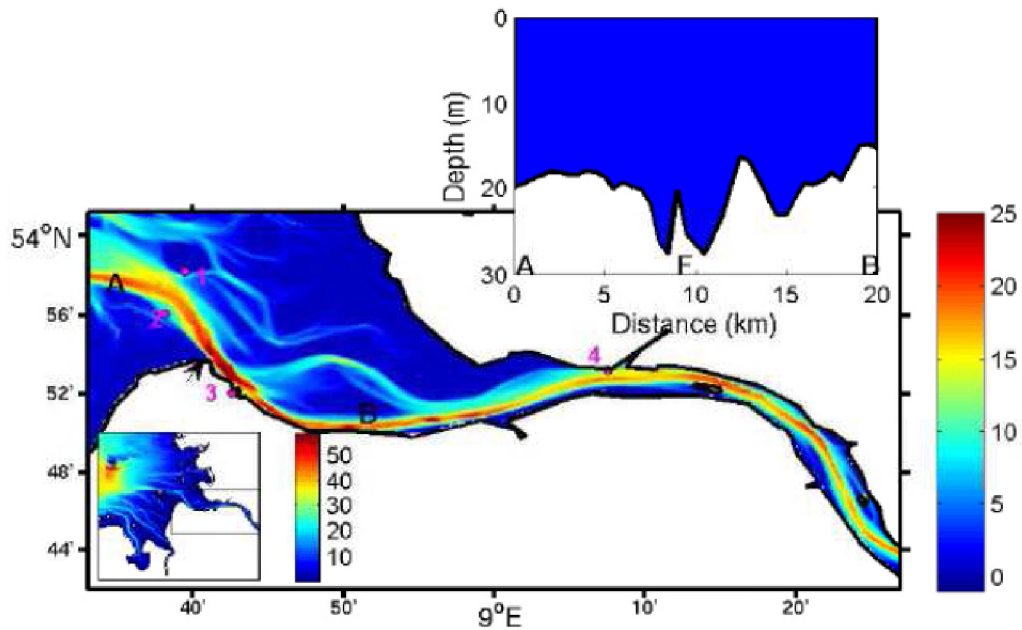
Figure 41. Geographic location of Elbe estuary and the bathymtery with locations of the 4 tide gauge data. The vertical profile shows along channel distance versus depth with letter A, B indicating the track along channel and letter F showing the front position.

The correlations of the observation data with model of amplitude and phase are presented in Figure 42. The results show the 200m resolution is clearly capable to improve M2 amplitude and phase model results compared to 400m. This is due to the fact that 200m GETM circulation model has high enough spatial resolution to capture propagation, coastal geometry and eddy processes. These processes play a key feature of bottom topography and ocean dynamic exchange.
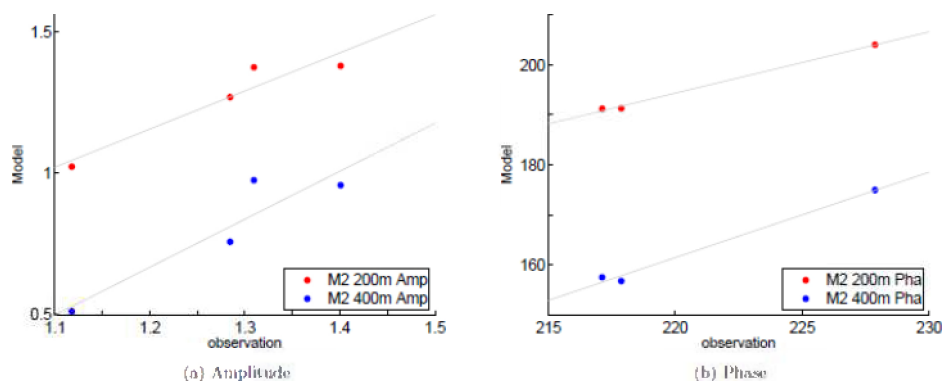
Figure 42. Amplitude (a) and phase (b) comparison between observation data and model results (blue: 400m spatial resolution, red: 200m) at four stations in the Elbe estuary.

This result gives confidence for using higher resolution for future studies in purpose of resolving complex upstream geometry features.

3.5.   Gulf of Venice

The aim of this section is to discuss impacts of the imposed boundaries on ocean circulation and sediment dynamics in the Gulf of Venice, the northernmost part of Adriatic Sea (Figure 43). To this end, atmosphere/land forcings and seabed/lateral boundary conditions have been studied by using a 3-D ocean-wave coupled modelling system (Ocean–Atmosphere–Wave–Sediment Transport, COAWST) forced by a high-resolution atmosphere model (COSMO-I7). COAWST relies on the ocean model ROMS (Regional Ocean Modeling System), the wave model SWAN (Simulating WAves Nearshore), and the CSTMS (Community Sediment Transport Modeling System) routines. The two-way data transfer between circulation and wave models was synchronous via Model Coupling Toolkit (MCT).
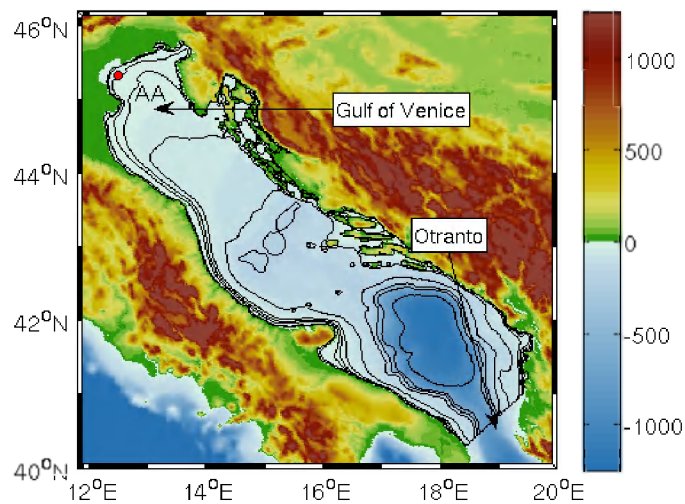
Figure 43. Adriatic Sea bathymetry and the northern Gulf of Venice. The AA marker shows the Acqua Alta platform location.

COAWST system has been implemented in the Adriatic Sea for a 12-month hindcast period, ranging from 2010 September, 1 to 2011 August, 31, and it was based on two different curvilinear orthogonal computational grids. The coarse parent grid (with horizontal spacing of 2.0 km in both directions, and 20 vertical sigma-levels) covers the whole Adriatic Sea, locating the southern open boundary at the Otranto Strait (Figure 43). The adopted child grid has horizontal spacing of 0.5 km, and it was offline nested to the parent grid in the northern Adriatic Sea sub-region (Gulf of Venice, see Figure 44). The two-way coupled system (referred as 2WC) that included the transfer of forcing terms between ROMS and SWAN was used in both parent and child grids. To assess the influence of coupling, on the fine grid the uncoupled COAWST system (referred as UNC) was also run for the winter season from January 1st to March 31st, 2011.
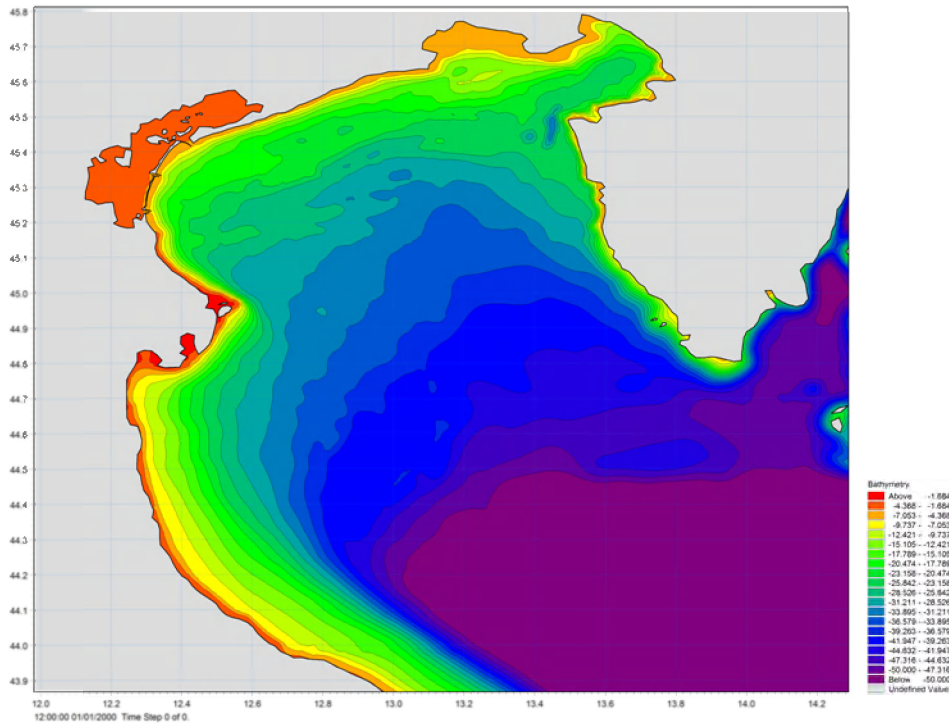
Figure 44. Gulf of Venice detailed bathymetry.

At the Otranto strait, ROMS open boundary conditions (sea surface elevation, vertical distribution of 2-D momentum, temperature and salinity; see Figure 45 and Figure 46) were taken from the Mediterranean Forecasting System (MFS) running at INGV (Istituto Nazionale di Geofisica e Vulcanologia), released through MyOcean service (http://www.myocean.eu.org/). Along this boundary five tidal constituents were imposed (namely, M2, S2, N2, O1, K1), as obtained through the Oregon State University (OSU) model (http://volkov.oce.orst.edu/tides/). For ROMS, initial conditions of 3-D velocity, 2-D velocity, sea surface height, temperature and salinity were obtained from an operational version running at the University of Ancona.
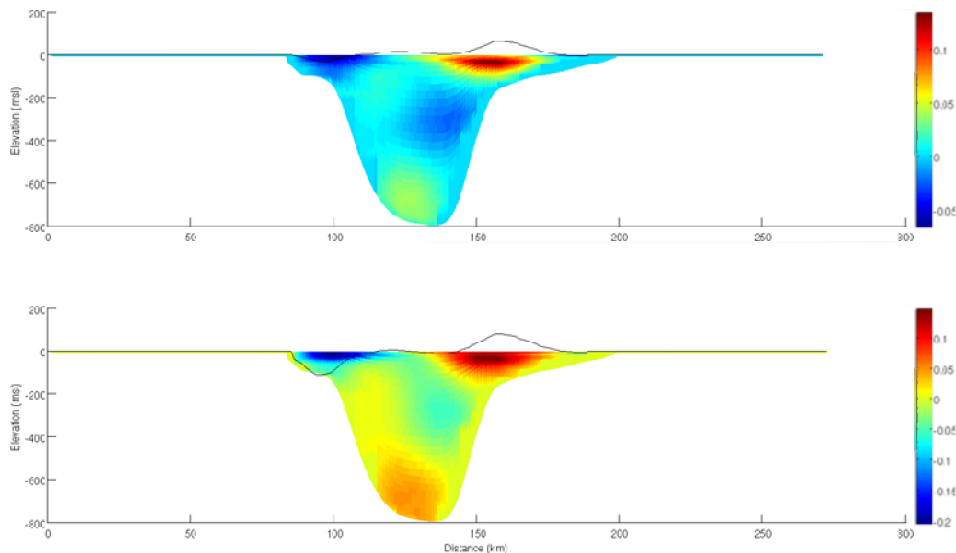
Figure 45. MFS boundary conditions at Otranto Strait. Example of 2-D and 3-D momentum (m/s).
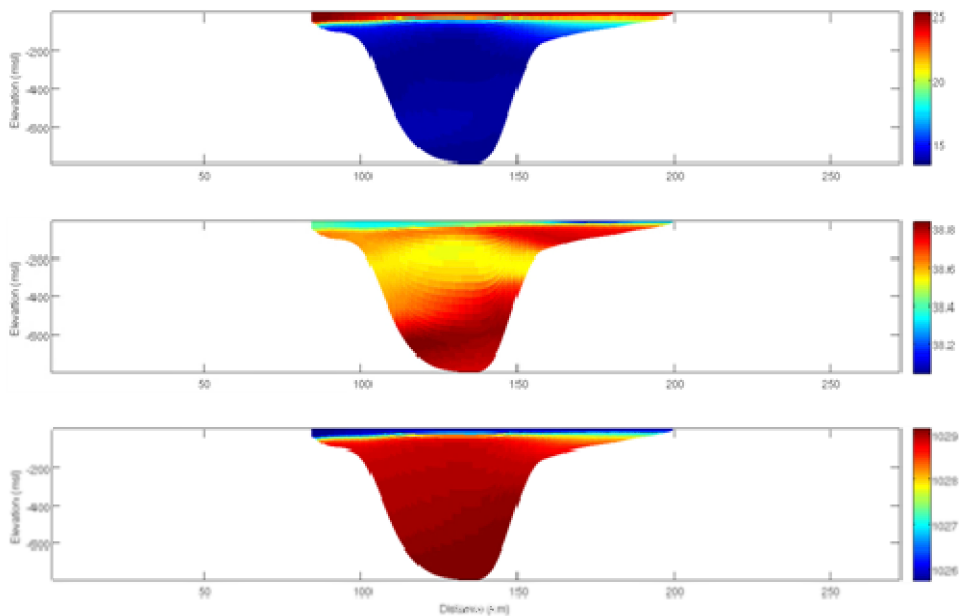
Figure 46. MFS boundary conditions at Otranto Strait. Example of Potential Temperature (°C), Salinity (PSU), and Density (kg/m³).

For the whole hindcast period on the coarse grid (September 2010-August 2011), wind and waves were recorded at the ISMAR-CNR Acqua Alta tower, located in the northern Adriatic Sea (Lat = 45° 18' 83" N, Lon = 12° 30' 53" E, see Figure), where local water depth is approximately 16 m. In addition to Acqua Alta data, to analyze model predictions Jason-1 (NASA \ CNES), Jason-2 (NASA \ CNES \ EUMETSAT \ NOAA), and Envisat (ESA) remotely sensed significant wave height H_s and U_{10} were also considered. Figure 47 illustrates a 3-month time series comparison of modeled and observed U_{10} at Acqua Alta. Within the period shown, all the peaks correspond to

Bora events, except one Sirocco wind condition. The COSMO-I7 model captures the timing of the wind events, and there is no clear evidence of a magnitude reduction. Indeed, within the period shown in Figure 47, Bora and Sirocco events that occurred with peak speeds greater than 10 m/s were well predicted. The same behavior is shown by the H_s a time series (Figure 48), but with a smoother field.
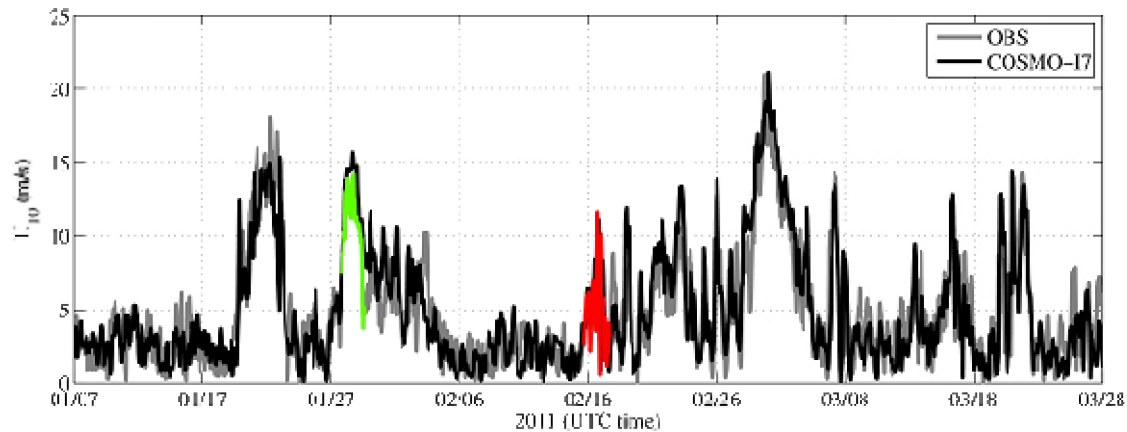
Figure 47. Time series comparison of modeled (COSMO-I7) and observed (OBS) wind speed U10 at the oceanographic tower Acqua Alta. Example of Bora (green line) and Sirocco (red line) wind events are highlighted.
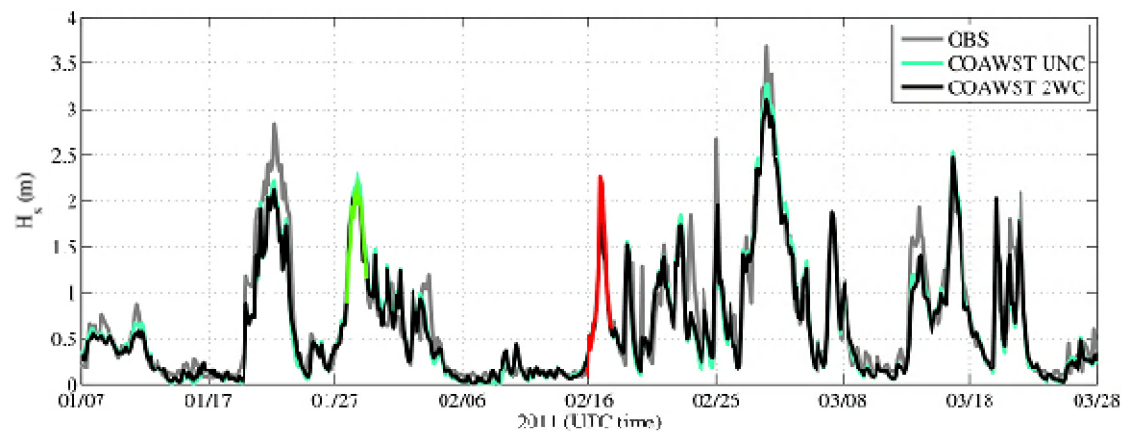
Figure 48. Time series comparison of modeled (COAWST) and observed (OBS) significant wave height Hs at the oceanographic tower Acqua Alta. Simulated Hs are shown as computed by the fully coupled (2WC) and uncoupled (UNC) systems. Example of Bora (green line) and Sirocco (red line) wave events are highlighted.

Land run-off has been incorporated in COAWST setup, accounting for water discharge, tracers (temperature and salinity), and sediments supply from main rivers tributary to the Adriatic Sea (Table 5). In ROMS, rivers are implemented as point source with a 3-D structure of the discharge, that we assumed to be uniform along the vertical direction. A different number of vertical layers has been considered, discretizing the water depth with 20 and 12 sigma-layers, for the parent and child

grids, respectively. Daily-averaged time series of fresh water and sediment concentration supplies from the Po river were imposed. In order to better account for the impact on coastal circulation and sediment supply, the flow of other rivers based on monthly-mean values using climatological estimates were also imposed, for a total of 26 rivers.

Name	Longitude	Latitude
Drin	19.371855	41.845398
Neretva	17.441067	43.017302
Isonzo	13.560475	45.718827
Tagliamento	13.111067	45.629332
Piave	12.728046	45.526914
Brenta	12.318243	45.185480
Adige	12.337650	45.164323
PO Pila	12.553622	44.970094
PO Tolle	12.480747	44.872236
PO Gnocca	12.421103	44.809758
PO Goro	12.399900	44.791350
PO Maestra	12.410936	45.036681
APE Reno	12.281101	44.593426
APE Foglia	12.906417	43.925918
APE Metauro	13.0558	43.8297
APE Esino	13.372704	43.645289
APE Musone	13.643138	43.474175
APE Potenza	13.672153	43.423204
APE Chienti	13.743317	43.293793
APE Tronto	13.917606	42.894464
APE Pescara	14.230748	42.470534
APE Sangro	14.543689	42.235937
APE Trigno	14.798497	42.065496
APE Biferno	15.028589	41.979409
APE Cevaro	15.894728	41.583890
APE Ofanto	16.198465	41.362048

Table 5. Adriatic Sea rivers (name and geographical position) used in COAWST.

The seabed boundary condition analysis focused on the analysis of sediment dynamics, bottom shear stresses, and suspended sediment concentration. A comparison was performed between the results of 2WC and UNC runs over the 2011 winter season (January 01 to March 31, 2011), especially considering two storms driven by the dominant winds blowing on the basin, Sirocco and Bora. During the Bora event compared to UNC, 2WC run provides an average increase of the total bottom shear stress in the offshore zones of the circulation pathways, while in shallower waters, towards the western Adriatic coast, a decrease in the same quantity has been found. Indeed, wave group velocity and currents generated during this storm are nearly parallel and concordant, especially in the northernmost part of the basin. In this framework, the currents are enhanced by momentum injections from waves, which are, in turn, elongated and lowered: as a consequence, current-generated stresses are increased and wave-generated ones are reduced, and the overall result depends on the local relative weight of these two factors. This can clearly be seen at AA, where the

wave contribution largely overwhelms the current stress giving rise to a higher maximum in the uncoupled simulation (Figure 49). A similar behavior has been found along the whole western Adriatic coast and in all the shallow zone between the Po delta and the Soča Estuary. Eastwards, in the Gulf of Trieste, the limit imposed by the short Bora fetch allows the currents to give a significant contribution to the total bottom stress.
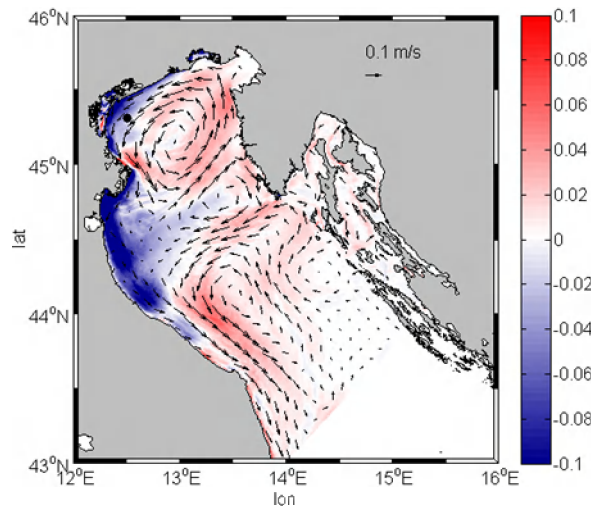
Figure 49. Bora storm. Storm-averaged maximum bottom stress: difference between 2WC and UNC runs. Black arrows show the storm- and depth-averaged current velocity from the 2WC run. Black dot shows the AA tower position.

3.5.1. Discussion, limitations and uncertainties

The analysis performed allowed to focus of different aspects concerning fluxes and boundary conditions in a basin where currents and waves are combined in a coupling framework. On the free-surface, fluxes analysis revealed errors smaller than 10 % and 20 % for wind magnitude and significant wave height, respectively, clearly indicate a trend of increased quality of atmospheric forcings. This is much more important in an area like the Adriatic Sea where the mountain ridges surrounding the basin induce a topographic effect into the wind field blowing on the water surface.

In presence of a coupling between ocean model and wave model, the atmospheric boundary layer in the wave model effects of ocean currents are accounted for by using the apparent local wind speed and direction to modify the wind stress. The wind speed modification by the local current is implemented in COAWST assuming the atmosphere flow relative to a moving frame: the wind speed is shifted by the ocean current velocity. This hypothesis allows guessing from COSMO-I7 10-meter wind speed the effect of ocean current on surface stress.

The impact of boundary fluxes from land is highlighted during an event of high discharge supplied from Po river during 20th of March 2011.It was analyzed to identify the effect of wave-current

interaction on the 3-D structure of the fresh water supplied to the Sea. Figure 50 shows the depth-averaged salinity resulting from the coupled (2WC, left panel) and uncoupled (UNC, right panel) runs. At the time of river flood, winds blowing from North-East generated wave conditions propagating towards the Italian coast. The wave-induced momentum forced the salinity to remain confined close to the coast, with a less spreading of fresh water off shore. Similar effect was observed on the 3-D structure of the salinity extracted in a computational point in front of the Po river main mouth (Figure 51). The role of the wave action is to confine fresh waters close to the coast, whereas they are free to mix with ocean salt water when the wave effect is not taken into account.
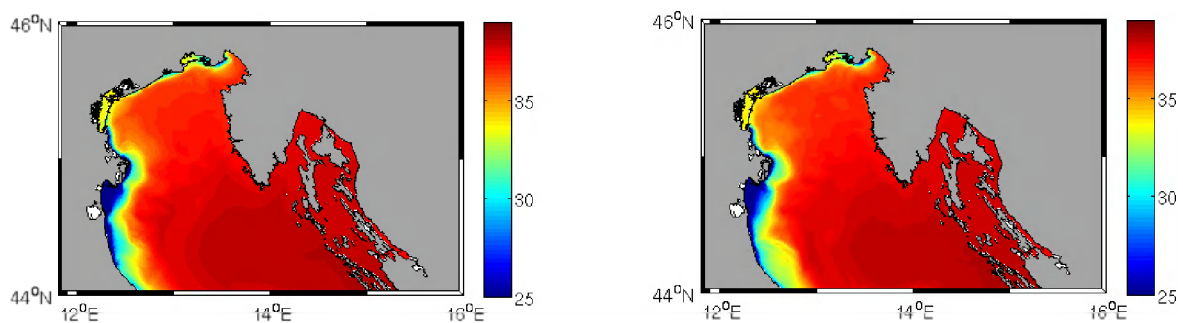
Figure 50. COAWST runs in the Gulf of Venice (20th March, 2011):Depth-averaged sea salinity. Coupled (2WC, left) and uncoupled (UNC, right) runs.
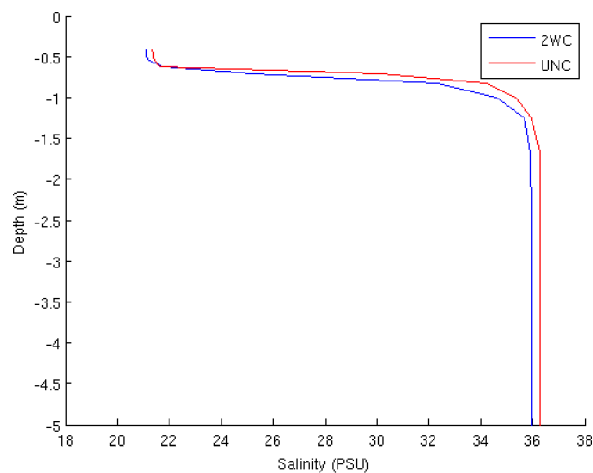
Figure 51. COAWST runs in the Gulf of Venice (20th March, 2011): water salinity vertical profile in front of Po river.

At the sub-basin scale, the description of global circulation provides a deeper insight on the advective dynamics leading to the aforementioned resultson seabed stresses. The coupling of waves and currents results in an increase in current speed of the order of about 0.10 m/s, enhancing the two

bathymetry-driven cyclonic gyres acting in the gulf of Venice and southwards of the Po delta respectively. As a consequence of such a flow field, a spyral-shaped pattern of suspended sediment (mostly suspended in the northern coast of the basin) arises in the northernmost end of the basin (Gulf of Venice), and the enhanced velocity of the coupled system produces a widening in the gyre arms, thus transporting the sediment cloud closer to the coastline. More precisely, on March 2nd at 9.00 AM the westernmost front of the sediment spiral momentarily reaches the Acqua Alta Tower in the coupled simulation giving rise to the first concentration peak (0.12 kg/m3), while in the uncoupled one it remains confined several kilometres further offshore. A new concentration maximum occurs 33 hours later in the 2WC run, when AA is reached by the tail of the spiral arm. In the meantime, in the UNC run the peripheral region of a much more compact sediment vortex starts approaching AA, generating a concentration peak on March 5th, at 00 PM (Figure 52). South of the Po delta, where circulation dynamics are less active and the effect of wave-current interactions is weaker, the UNC and 2WC simulations show very similar stories, with minor differences concentrated along the circulation pathway flowing westwards from the Kwarner Gulf and south-eastwards along the western Adriatic coast.
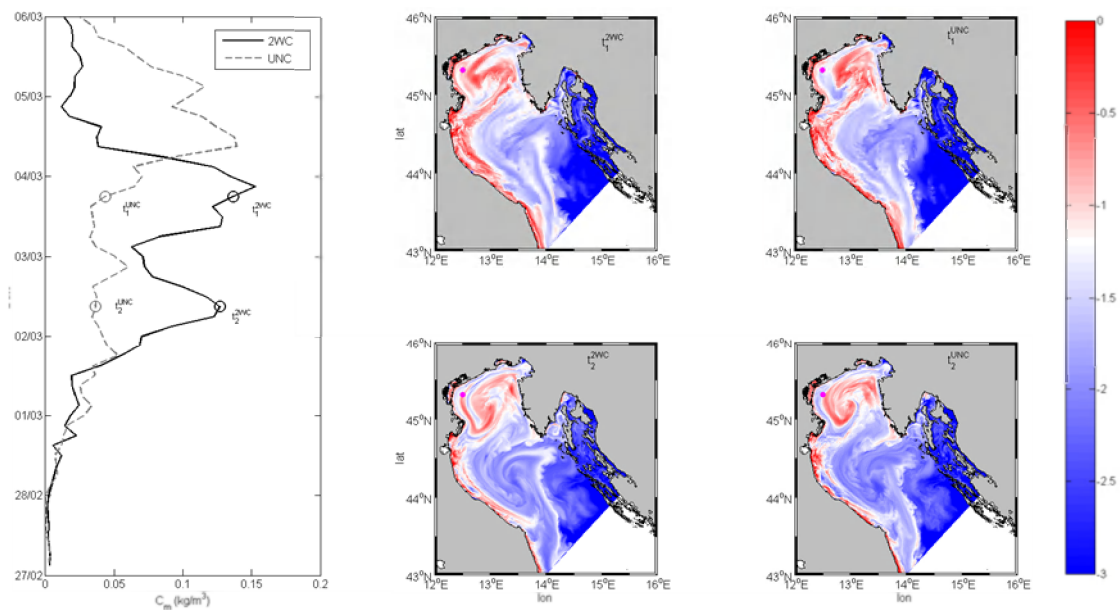
Figure 52. Gulf of Venice suspended sediment concentration (log10 kg/m3) patterns in the 2WC (left panels) and UNC (right panels) runs during the Bora storm. Top: conditions at 2nd March, 2011 (09:00 AM). Bottom: conditions at 3rd March, 2011 (18:00 PM). The dot marks the position of the Acqua Alta Tower. The depth-averaged sediment concentration (kg/m3) at AA is shown on the left hand of the Figure, where circles show the time (t1 and t2) of sediment conditions depicted.

4. Discussion and Conclusions

Coastal ocean regions are dynamic and complex environments that are driven by an intricate interaction between atmospheric, oceanographic, estuarine/riverine and land–sea processes (Smith et al., 2010). The present study is motivated by the need to establish and use the best possible boundary conditions for coastal water quality modelling. For this reason, improvements to boundary fluxes during the Field_Ac project is described. The description of the improvements is followed by examples of the impact of improved boundary conditions at the study sites; i.e. the Catalan coast, Liverpool Bay, German Bight and Gulf of Venice.

Improvements to boundary fluxes from land:

Improvements in predicting land boundary fluxes (covered in Report D3.1):

For the land boundary side the needed products are distributed and point wise run-off both quantitatively and qualitatively has been solved. On the one hand, the Report D3.1 "Methodology (including best practice guidelines) on how to identify and incorporate 'concentrated' and 'distributed' run-off in pre-operational forecasts, based on the input and requirements from our users" (Keupers et al., 2011) lists in detail the data needs regarding precipitation, evapotranspiration, digital elevation model, land use, and observations of discharges and water quality. It also explains rigorously how a conceptual model can be set up to predict river runoff (Figure 1) and urban drainage overflow (Figure 2) that can be incorporated into coastal scale oceanographic models.

Improvements in incorporating the continental runoff into the coastal waters (covered in D3.2):

On the other hand, the needs to understand and predict the phenomena that control the fate of freshwater after their release in the coastal ocean have been studied by KU Leuven. The main improvements corresponding to continental runoff are detailed below:

- Incorporate the continental runoff into the coastal waters.
- Incorporate combined sewer overflows (CSOs) into the coastal waters.
- Tested different vertical profile structures of the continental discharge.

Improvements to free-surface boundary condition:

For the atmospheric boundary, products from local scale meteorological models (wind, atmospheric pressure and rainfall) are needed. In order to improve meteorological simulations to provide the meteorological information required by the oceanography modellers, several implementations have

been tested by BSC: high spatial resolutions, data assimilation of Sea Surface Temperature (SST) from MyOcean, physical parameterizations and nesting options.

Other implementations have been tested by NOCL. Weather Forecasting and Research model (WRF) has been implemented at 12, 4, and 1.3km resolution for a storm event over the Irish Sea (Bricheno et al. 2012). The outputs were used to force the coupled hydrodynamic and wave model POLCOMS-WAM and the effect on storm surge and waves has been assessed. An improvement was observed in the WRF model pressure and wind speed when moving from 12km to 4km resolution with errors in wind speed decreasing more than 10% on average. When moving from 4km to 1.3km no significant further improvement was observed.

Sensitivity to frequency of meteorological forcing was tested in this configuration, at 1, 3, 6, and 12 hourly rates. Lower wave heights were found when applying lower frequency wind forcing. Reducing to the frequency to 3 hourly decreases the mean wave height by around 4cm and the maximum by an average of 13cm. The most extreme differences between using 12 hourly and 1 hourly forcing can be as much as 2m difference in the interior of the Southern Irish Sea. Connected work by O'Neill et al. (2012) investigates model sensitivity of shelf sea surface properties to frequency of meteorological forcing.

Brown and Wolf (2009) investigated whether a wave-dependent surface drag is useful for accurate surge prediction, and also if this can be represented by an optimised Charnock parameter. They concluded that including a wave-dependent Charnock parameter removes the need to find an optimized constant value for different sea areas and model resolution, and will provide an acceptable prediction across the eastern Irish Sea for different surge events.

Improvements to seabed boundary condition:

For the seabed, boundary information on sediment composition, bedforms and bathymetry and bio-geo-chemical parameters is essential. Depending on the complexity of the numerical model, various types of bottom boundary conditions are required for the hydrodynamic equations and sediment transport equations.

KU Leuven has provided an overview of current practises, focused on a new strategy based on much more physical insight (physical roughness, drag modulation by suspended sediment and low-Reynolds drag law) and less on empiricism to supply bottom boundary conditions for hydrodynamic modelling (for 2DH and 3D hydrodynamic models) and to bottom boundary conditions for sediment transport modelling (2DH and 3D sediment transport models). With the

new modelling strategy where the low-Reynolds layer is explicitly computed using the GML theory, the sought-after reference concentration in the near-bottom node is computed by numerical integration of the transport in the low-Reynolds layer. Again, it is preferred to explicitly impose this concentration as an essential (Dirichlet) boundary condition, since the interpolation functions are not adequate enough to approximate the true concentration profile over the low-Reynolds layer. An application test case has been developed (and applied to the Western Scheldt sediment budget).

In regional scales it is difficult to resolve the gradients in velocity and the bottom boundary layer.. LIM/UPC developed and used multiple algorithms to solve de Bottom Boundary Layer (BBL) that consider both effects of wave and current action on bottom shear stress (e.g.: Styles and Glenn, 2000; Soulsby, 1995; Blaas et al., 2005; Warner et al, 2008). These complex routines simulate BBL processes in the presence of waves and mobile sediment. The short (order-10 s) oscillatory shear of wave-induced motions in a thin wave-boundary layer produces turbulence and generates large instantaneous shear stress (Warner et al., 2008). As example, nested coupled-models in Catalan coast have allowed to determine spatially the prevalent processes in the regionshowing wave-dominated or current-dominated beds.

HZG performed several sensitivity experiments to study the response of the German Bight circulation with several bottom roughness configurations. The differences in the bottom salinity were more pronounced in the coastal areas (the offshore deeper areas were not so sensitive to bottom roughness variations).

In order to assess the importance of the seabed boundary layer and the consequent energy dissipation due to bottom friction in a spectral wave model applied to the inner shelf, the performance of the use of the JONSWAP bottom friction dissipation source term has been compared to the use of the model BT4 (Ardhuin (2001)) by SHOM. The validation with altimeter data and buoys has shown a small improvement of the results in the North Sea along the French and the Belgian coast. BT4 needed some improvement to clearly demonstrate its efficiency on a heterogenic bottom and mobile sediment. Such effects cannot be taken into account in the JONSWAP parameterization. The relative success of using a constant value for the coefficient in the JONSWAP formulation, although there is no real physical justification, may be explained by the fact that it describes qualitatively the decrease in bottom drag with increasing forcing expected on a movable bed (Ardhuin et Al., 2003). The JONSWAP model leads to overestimation of wave dissipation over relic ripples and does not describe the sharp increase of bottom roughness where

active generation of ripples is expected. The model BT4 doesn't take into account the tidal currents that should play an important role in the degradation and formation of ripples and also the presence of current should influence the wave boundary layer. But the available model using currents, like the Grant & Madson one, have been reported by Tolman (1991) to generate opposite effects to those recorded by measurements. The BT4 model should be extended to the mud and sand mud mixture to fully reproduce the nature of the bottom.

Improvements to open boundary condition:

For the open boundary condition 3D current and water quality fields and wave spectra are used (from MCS ocean and shelf scale products).

Various approaches to the specification of open boundary fluxes are used in the FIELD_AC project:

  (i) Use of MyOcean data.

  (ii) Use of nested models: most partners are running nested model grids.

  (iii) Use of unstructured grids: the combination of a continuous increase in the power of available computing facilities, together with an interest in modelling sea areas close to complex coastal boundaries means that the flexibility provided by unstructured mesh modelling is proving to have many advantages.

For the pre-operational modelling suite run at NOCL, POLCOMS presently receives boundary data from the UK Met Office FOAM global ocean model. The FOAM model will be discontinued at the end of December 2012, and the plan is to replace the boundary forcing with a new product derived from MyOcean, FOAM-AMM7. The Forecasting Ocean Assimilation Model 7km Atlantic Margin model (FOAM AMM7) is a coupled hydrodynamic-ecosystem model, nested in a series of one-way nests to the Met Office global ocean model. The hydrodynamics are supplied by the Nucleus for European Modelling of the Ocean (NEMO) with an Optimal Interpolation (OI) data assimilation scheme for sea surface temperature. This is coupled to the European Regional Seas Ecosystem Model (ERSEM), developed at Plymouth Marine Laboratory (PML). The current products available from the MyOcean data portal are too low resolution in both time and space for model downscaling, but work in ongoing to access the full output of the NEMO model.

LIM/UPC has used the MyOcean products for the oceanographic boundary conditions and atmospheric forcing in the Catalan Coast. In essence, the products used correspond to the Mediterranean Forecasting System running at INGV. This uses an OGCM (Ocean General Circulation Model) off-line coupled with a wave model and the OCEANVAR data assimilation

scheme. It is running every day providing 10 days of forecast and once a week (on Tuesday) 15 days of analysis for the 3D physical ocean. The grid resolution is 1/16 x 1/16 degree and 72 unevenly spaced vertical levels. The variables used in this case correspond to Salinity, Temperature, Sea Surface height, Zonal Velocity and Meridional Velocity. The interpolation to the domain is done using objective analysis for the "father-masked" areas and conservation flow correction at the boundaries. Alternatively, some tests are actually being carried out with winds from another data source (e.g. MeteoCat, BSC, measured data, etc.). After a comparison of measured data and Catalan coast, it is suggested to increase the temporal resolution of Myocean products, in particular the sea surface height, which are associated with pressure gradients, that jointly with the local windhave an important influence in the shelf dynamics in the Catalan area.

Impacts of improved boundary conditions at study sites

Catalan Coast

In this case study the impact of the introduction of land boundary fluxes on the hydrodynamics of coastal waters and the relative importance of different freshwater discharges of the plume and the role of land boundary fluxes in determining the structure of the plume is shown. For this, a 3D hydrodynamical model (ROMS) has been set up to incorporate the continental and urban run-off into the Catalan Coastal waters. The results were used by KU Leuven to examine the dispersal to a freshwater delivery from two relevant events; a low river discharge typical of mean conditions during April 11th 2011 and a high discharge representative of the storm event during March 17th 2011 from several points of view:

    i.   Impact to freshwater into the coastal waters

    ii.   Impact to CSO's into the coastal waters

    iii.   Impact to different freshwater flows into the coastal waters

    iv.   Impact to different vertical profiles into the coastal waters

On the other hand, different impacts related to surface boundary conditions (atmospheric modelling) were studied for the Catalan Coast by BSC:

    i.   Impact of high spatial resolution

    ii.   Impact to assimilation of Sea Surface Temperature (SST) at high spatial resolution

    iii.   Impact to different physical parameterizations

    iv.   Impact to nesting options

Liverpool Bay

The impact of the atmospheric boundary and bottom friction has been analyzed by NOCL in this case study. Some quite general comments can be made: As NOCL downscale to finer and finer resolution, the boundary forcing becomes more dominant, and the local forcing more important. Including sufficient physics in the boundary forcing will give better performance in small scale models. Two examples of this are:

- Including baroclinic effects, e.g. tidal modulation of wave heights is observed in very shallow waters in Liverpool Bay.
- Including boundary waves (not provided by MyOcean) is needed to get the full wind and swell signal.

The resolution of boundary forcing in both time and space is also very important, as shown by the example of high resolution winds. In an experiment for downscaling and coastal forecasting, it was apparent that the model using more frequently available boundary conditions outperformed the model performance using the currently available MyOcean boundary conditions.. In this experiment FOAM provided boundary conditions for the AMM model, which in turn forced the open boundary of the Irish Sea domain. These are not official Met Office products but were supplied to NOCL on a "best endeavour" basis. This experiment illustrated that improvements to the standard MyOcean products could be made.

German Bight

The assessment of the impact of improved boundary conditions in the German Bight was studied from several points of view:

i. The role of the meteorological forcing, extreme events

ii. The role of the atmospheric forcing

iii. Incorporation of Land Discharge Runoff into Oceanographic Models

iv. Role of the atmospheric forcing and density stratification

v. Impact of MyOcean open boundary conditions

vi. Impact of high resolution wind forcing

vii. Impact of wave forcing on hydrodynamic modelling results

viii. Impact of higher resolution on estuarine modelling

Gulf of Venice

Impacts of the imposed boundaries on ocean circulation and sediment dynamics in the Gulf of Venice, the northernmost part of Adriatic Sea were illustrated. To this end, atmosphere/land forcing and seabed/lateral boundary conditions have been studied by ISMAR-CNR.

The analysis performed allowed to focus of different aspects concerning fluxes and boundary conditions in a basin where currents and waves are combined in a coupling framework. On the free-surface, fluxes analysis revealed errors smaller than 10 % and 20 % for wind magnitude and significant wave height, respectively, clearly indicate a trend of increased quality of atmospheric forcings.

When the ocean model and wave model are coupled, the atmospheric boundary layer in the wave model effects of ocean currents are accounted for by using the apparent local wind speed and direction to modify the wind stress. The impact of boundary fluxes from land is highlighted during an event of high discharge supplied from Po river during 20th of March 2011. It was analyzed to identify the effect of wave-current interaction on the 3-D structure of the fresh water supplied to the Sea. At the time of river flood, winds blowing from North-East generated wave conditions propagating towards the Italian coast. The wave-induced momentum forced the salinity to remain confined close to the coast, with a less spreading of fresh water off shore.

5. Bibliography

Ardhuin F., T.H.C., Herbers and W.C., O'Reilly. (2001). A Hybrid Eulerian–Lagrangian Model for Spectral Wave Evolution with Application to Bottom Friction on the Continental Shelf. *Journal of physical oceanography*, Vol. 31, pp. 1498-1516.

Ardhuin, F, W.C. O'Reilly, T.H.C. Herbers, and P.F. Jessen. (2003). Swell transformation across the continental shelf. Part I: Attenuation and directional broadening. *J. Phys. Oceanogr*, Vol. 33, pp.1921–1939.

Bagnol, RA. (1946). Motion of wave in shallow water ; Interaction between waves and sand bottoms. *Proc. Roy. Soc. London A*, Vol. 187, pp.1-18.

Bagnold, R.A. (1946). Motion of waves in shallow water, Interaction between waves and sand bottom. *Proc, Royal Society London,*, Vol. 187, pp. 1-15.

Beach, R.A., and R.W.,Sternberg. (1992). Suspended sediment transport in the surf zone: response to incident wave and long-shore current interaction. *Marine Geology*, Vol. 108, pp. 275–294.

Blaas, M., C., Dong, P., Marchesiello, J.C., McWilliams, K.D., Stolzenbach. (2005). Sediment-transport modeling on Southern Californian Shelves: a ROMS case study. . *Continental Shelf Research* , Vol. 27, pp. 832–853.

Bolaños, R., P., Osuna, J., Wolf, J., Monbaliu and A. Sanchez-Arcilla. (2011). Development of POLCOMS-WAM model. *Ocean Modelling*, Vol. 36 (1-2), pp. 102-115.

Booij, N., R.C., Ris, L.H., Holthuijsen. (1999). A third-generation wave model for coastal regions: 1. Model description and validation. *Journal of Geophysical Research*, VoL. 104, pp. 7649–7666.

Bouws, E., and G.J. Komen. (1983). On the balance between growth and dissipation in an extreme depth-limited wind-sea in the southern North Sea. *Journal of Physical Oceanography,* , pp. 1653-1658 .

Bricheno, L.M. and Wolf, J. (2011). *Practical criteria assessing the performance of structured versus un-structured grids and the various nesting configurations.* Report.

Bricheno, L.M., A., Soret, O., Jorba, J., Wolf and J., Baldasano. (2012). Effect of high-resolution meteorological forcing on nearshore wave and current model performance. Submitted to JAOT. *Submitted to JAOT.*

Brown, J.M. (2010). A case study of combined wave and water levels under storm conditions using WAM and SWAN in a shallow water application. *Ocean Modelling*, Vol. 35 (3), pp. 215-229.

Brown, J.M. and J. Wolf. (2009). Coupled wave and surge modelling for the eastern Irish Sea and implications for model wind-stress. *Continental Shelf Research*, Vol. 29, pp. 1329–1342.

Brown, J.M., R. Bolaños and J., Wolf. (2011). Impact assessment of advanced coupling features in a tide-surge-wave model, POLCOMS-WAM, in a shallow water application. *Journal of Marine Systems*, Vol. 87, pp. 13-24.

Carbajal, N. and T., Pohlmann . (2004). Comparison between measured and calculated tidal ellipses in the German Bight. *Ocean Dydamics*, Vol. 54, pp. 520-530.

Cellino, M. (1998). *Experimental study of suspension flow in open channels.* Ph.D.dissertation, Dept. of Civil Engineering, Ecole Polytechnique Fédérale de Lausanne, Lausanne, Switzerland.

Emeis, S. and M., Türk . (2009). Wind-driven wave hights in the German Bight. *Ocean Dynamics*, vol. 59, pp. 463-475.

(n.d.). *Field_AC project.* (http://www.field_ac.eu). EU- FP7-SPACE-2009-1-242284.

Garlan T. (n.d.). Innovation in marine cartography at SHOM. . *International Hydrographic Review, LXX(1).*

Grant W.D. and O.S., Madsen . (1982). Movable bed roughness in unsteady oscillatory flow. *Journal of Geophysical Research*, vol. 87, pp. 469-481.

Hasselmann, K., Barnett, T.P., Buows, E., Carlson, H., Cartwright, D.E., Enke, K., Ewing, J.A., Gienapp, H.,Hasselmann, D.E., Kruseman, P., Meerburg, A., Mu¨ller, P., Olbers, D.J., Richter, K., Sell, W., Walden, H. (1973). Measurements of wind-wave growth and swell decay during the Joint North Sea Wave Project JONSWAP. In *Deutsches Hydrographische Zeitschrift* (pp. 8 (12)., 95, Suppl. A.).

Kajiura, K. (1968). *A model of the bottom boundary layer in water waves.* Bull. Earthquake Res. Inst., Univ. Tokyo, 46, 75–123.

Keupers, I., P. Willems, J. Fernandez Sainz, L. Bricheno, J. Wolf, J. Polton, J. Howarth, S. Carniel, and J. Staneva. (2011). *Methodology (including best practice guidelines) on how to identify and incorporate 'concentrated' and 'distributed' run-off in pre-operational forecasts, based on the input and requirements from our users.* Field_AC project (EU-FP7-SPACE-2009-1-242284).

Kourafalou V.H, Oey L.Y., Wang J.D and Lee T.N. (1996). The fate of river discharges on the continental shelf. 1. Modeling the river plume and the inner shelf coastal current. *Journal of Geophysical Research*, Vol. 101, pp. 3415-3434.

Krone, R.B. (1962). *Flume studies of the transport of sediment in estuarial shoaling processes.* Final report. Hydraulic Eng. Laboratory & Sanitary Eng. Research Laboratory, University of California, Berkeley (CA).

Kundu, P.K. . (1976). Ekman veering observed near the ocean bottom. *J Phys Oceanogr* , Vol. 6, pp. 238–242.

Liste, M., J. Monbaliu, M. Grifoll, M. Espino, I. Keupers, S. Carniel, A. Benetazzo, M. Sclavo, J. Staneva, L. Bricheno, and J. Wolf. (2011). *Methodology to introduce the 3D boundary condition for river discharges (including practical recommendations) for the 4 studied sites as a function of their prevailing conditions and users needs.* Field_AC project (EU-FP7-SPACE-2009-1-242284).

Madsen, J., Detrick, R., Mutter, J., Buhl, P. and Orcutt, J. . (1990). A two- and three-dimensional analysis of gravity anomalies associated with the East Pacific Rise at 9N and 13N. *Journal of Geophysical Research*, Vol. 95 (B4).

Madsen, O.S. (1994). Spectral wave-current bottom boundary layer flows. *Proceedings 24th International Conference on Coastal Engineering, ASCE, Kobe* , (pp. 1:384-398).

Madsen, O.S., and P.N., Wikramanayake. (1991). *Simple models for turbulent wave-current bottom boundary layer flow.* U.S. Army Corps of Engineers. WES, Report No. DRP-91-1.

Madsen, OS., Y.K. Peon and H.C. Graber. (1988). Spectral wave attenuation by bottom friction: theory. *Proc. 21st Int. Conf. Coastal Eng., Malaga. ASCE,* (pp. pp. 492-504).

(n.d.). *MyOcean products .* (http://www.myocean.eu/).

Nielsen, P. (1981). Dynamics and geometry of wave-generated ripples. *J. Geophys. Res*, Vol. 86, pp. 6467–6472.

O'Neill C.K., J.A., Polton, J.T., Holt, and E.J., O'Dea. (2012). Modelling temperature and salinity in Liverpool Bay and the Irish Sea: sensitivity to model type and surface sensitivity to model type and surface. *Ocean Sci. Discuss*, Vol. 9, pp. 649–685.

Polton, J. A., Palmer, M. R., & Howarth, M.J. (2011). Physical and Dynamical Oceanography of Liverpool Bay. *Ocean Dynamics*, Vol. 61 pp.1421–1439.

Shemdin, O., K., Hasselmann, S.V., Hsiao, and K., Heterich. (1978). Nonlinear and linear bottom interaction effects in shallow water. In: Turbulent Fluxes through the Sea Surface, Wave Dynamics and Prediction. *NATO Conf. Ser. V*, Vol. 1, pp. 347-365.

Shields, A. (1936). *Application of similarity principles and turbulence research to bed movement.* Hydrodynamic Lab. Rep. 167, California Institute of Technology, 43 pp.

Smith R.N., Chao Y., Li P.P, Caron D.A, Jones B.H, Sukhatme G.S. (2010). Planning and Implementing Trajectories for Autonomous Underwater Vehicles to Track Evolving Ocean.

Processes Based on Predictions from a Regional Ocean Model. *The International Journal of Robotics Research*, Vol 29. pp 1475.

Soulsby, R.L. (1995). *Bed shear-stresses due to combined waves and currents.* In: Stive, M.J.F. (Ed.). Advances in Coastal Morphodynamics: An Overview of the G8-Coastal Morphodynamics Project, Co-Sponsored by the Commission of The European Communities Directorate General XII, 4.20–4.23.

Styles, R., and Glenn S.M. (2000). Modeling stratified wave and current bottom boundary layers on the continental shelf. *JOURNAL OF GEOPHYSICAL RESEARCH*, Vol. 105, pp. 24,119 – 24,139.

Taylor P.K. and M.J. Yelland. (2001). The Dependence of Sea Surface Roughness on the Height and Steepness of the Waves. *J. Phys. Oceanogr*, Vol. 31, 572–590. .

Tolman, H. (1995). Subgrid modeling of moveable-bed bottom friction in wind wave models. *Coastal Eng*, Vol. 26, pp.57–75.

Tolman, H.L. (1991). A third-generation model for wind waves on slowly varying, unsteady and inhomogeneous depths and currents. *J. Phys. Oceanogr*, Vol. 21, pp. 782-797.

Tolman, H.L. (1992). An evaluation of expressions for wave energy dissipation due to bottom friction in the presence of currents. *Coastal Engineering*, Vol. 16, pp.165–179.

Tolman, H.L. (1993). An evaluation of expressions for wave energy dissipation due to bottom friction in the presence of currents-Reply to the discussion by Z.J. You. *Coastal Eng.*, Vol. 19, pp.329-333.

Tolman, H.L. (1994). Wind waves and moveable-bed bottom friction. *J. Phys. Oceanogr*, Vol. 24: 994-1009.

Toorman E.A. (2013). A Generalized Mixing-Length model for flow over rough surfaces. *in preparation.*

Toorman, E.A. & Q. Bi. (2013). *Bottom boundary conditions for hydrodynamics and sediment transport in hydraulic engineering software.* Report HYD/ET/FIELD_AC/2.4, Hydraulics Laboratory, KULeuven (in preparation).

Toorman, E.A. (2002). Modelling of turbulent flow with cohesive sediment. . *In: Proceedings in Marine Science, Vol.5: Fine Sediment Dynamics in the Marine Environment (J.C. Winterwerp & C. Kranenburg, eds.)* (pp. pp.155-169). Elsevier Science, Amsterdam.

Toorman, E.A. (2012). *Bottom boundary conditions for hydrodynamics and sediment transport in hydraulic engineering software.* Report HYD/ET/FIELD_AC/2.4, Hydraulics Laboratory, KULeuven .

Traykovski, P., A. E. Hay, J. D. Irish, and J. F. Lynch. (1999). Geometry, migration, and evolution of wave orbital ripples at LEO-15. *J.Geophys. Res.*, Vol. 104 (C1), pp. 1505–1524.

Trowbridge, J.H. and Y.C. Argrawal. (1988). Glimpses of a wave boundary layer. *Journal of Geophysical Research*, Vol. 100,pp. 20729–20743.

Warner, J.C., Armstrong, B., He, R. & Zambon, J.B. (2010). Development of a Coupled Ocean-Atmosphere-Wave-Sediment Transport (COAWST) modeling system. *Ocean Modeling*, 35(3), 230-244.

Warner, J.C., Sherwood, C.R., Signell, R.P., Harris, C. & Arango, H.G. (2008). Development of a three-dimensional, regional, coupled wave, current, and sediment-transport model. *Computers and Geosciences* , Vol. 34, pp. 1284-1306.

Widera, P., G., Ghorbaniasl and C., Lacor. (2009). Study of the sediment transport over flat and wavy bottom using large-eddy simulation. . *Journal of Turbulence*, Vol. 10(33), pp.1–20.

Wilson, K.C. . (1989). Friction of wave induced sheet flow. *Coastal Eng*, Vol. 12, pp. 371-379.